ANALYSIS AND DESIGN OF A SYNTHETIC APERTURE RADAR MEMBRANE ANTENNA

Etienne Ferland

Department of Mechanical Engineering
McGill University, Montreal

September 2005

A thesis submitted to McGill University in partial fulfilment of the requirements of the degree of Master of Engineering.

Abstract

Use of a membrane antenna on remote sensing satellites is now possible because of new materials and manufacturing technologies. This would allow space organisations to cut cost and weight by a non-negligible factor. All possible failure modes must be fully analyzed before these are sent to space. With membrane antennas, a new type of failure mode must be looked at: wrinkling. The wrinkling of the emitting layer could greatly undermine the performance of the antenna by modifying the orientation of the radiating elements rendering the wrinkle-affected area useless. It has been anticipated that such wrinkling could occur under temperature variations in space. There is currently a lack of available analyses for predicting with confidence the behaviour of such stretched material in a space environment. This work develops and establishes a finite-element approach as a potential method for predicting wrinkle height and orientation under thermal loads. Some designs for controlling the wrinkles are introduced with the benefits of optimizing the antenna area. The influence of the variation of the parabolic edges and corner cut-offs on the required cable load has been studied. Dynamic behaviour poses a concern, especially with a larger and flexible membrane and has been studied to determine the natural frequencies and the response of the antenna to on-orbit micro-vibrations.

Résumé

L'utilisation d'une antenne membrane sur les satellites de télédétection est désormais possible par la fabrication de nouveaux matériaux et le développement de nouvelles techniques manufacturières. Une telle antenne permettrait aux organisations possédant de tels satellites d'en réduire le poids et du fait même le coût de lancement par un facteur important. Toutes les causes d'échec, de panne ou d'insuccès reliées à l'utilisation d'une antenne membrane doivent être pleinement étudiées avant qu'elle ne soit lancée. Avec l'émergence de cette nouvelle technologie, une nouvelle problématique s'ajoute : le plissement. Le plissement de la membrane émettrice pourrait affecter l'efficacité de l'antenne et réduire ses performances électriques en modifiant l'orientation des éléments radiatifs de la membrane rendant ainsi inopérante la région affectée. Les variations de température présentes dans l'espace peuvent produire de tels plissements. Très peu d'analyses sont disponibles pour prédire en toute certitude le comportement d'une telle membrane en orbite. Cette étude propose l'étude d'une approche par éléments finis analysant la hauteur et l'orientation des plissements dues aux variations de température. Le contrôle des ridules par méthode passive a été également étudié permettant l'optimisation de l'aire et des dimensions de la membrane. L'influence de la forme parabolique des cotés de la membrane sur la force axiale du câble de tension a été étudiée et est présentée. Le comportement dynamique de la membrane est l'objet d'une attention particulière étant donné sa propension à amplifier les micro vibrations.

Acknowledgement

I would like to specially thank Arthur Baylis from EMS Technologies for giving me the opportunity to work with EMS Technologies and his team on a R&D project and establish collaboration for exchanging data and results to the benefit of all. My deep thanks and regards.

To Professor Arun Misra, I extend my profound gratitude and many thanks. His guidance has been continuous and particularly precious.

Also from EMS Technologies, I would like to thank Dino Keffalinos for his support and supplying the necessary information. To Steve Larouche and Dominick Lauzon for their insight, continuous interest and stimulating discussions, I would also like to extend my esteem and thanks.

Marie-Josée Potvin from the Canadian Space Agency has opened new avenues for this thesis by her interest, suggestions and collaboration. I am grateful.

And to Virginie Leblond for her unending support through this and much more.

TABLE OF CONTENTS

LIST OF FIGURES

LIST OF TABLES

NOMENCLATURE

α: Coefficient of thermal expansion (CTE)

ε: Strain

σ: Stress

ρ: Material density

υ: Poisson's ratio

ζ: Non-dimensional damping ratio.

d_1: Parabola depth of top and bottom membrane sides.

d_2: Parabola depth of left and right membrane sides.

e: Membrane corner edge length resulting from the corner cut-offs.

E: Modulus of elasticity or Young's modulus

k: Minimum distance between the electrical aperture corner and the corner edge.

l_o: Electrical aperture length.

l_a: Electrical aperture width.

l_1: Parabola length of top and bottom membrane sides.

l_2: Parabola length of left and right membrane sides.

Q: Quality factor where $Q \approx 1/2\zeta$.

t_1: Spacing between the electrical aperture and the closest point of the top and bottom membrane parabolic sides.

t_2: Spacing between the electrical aperture and the closest point of the left and right membrane parabolic sides.

1 INTRODUCTION

Many countries own one or more remote sensing satellites for scientific or military purposes. Remote sensing satellites are mostly operated to monitor or study global environment changes offering valuable information for future human activities. Remote sensing satellites use a wide variety of instruments and sensors such as infrared systems, imaging instruments, Synthetic Aperture Radar (SAR), spectrometers, radiometers, etc. These sensors enable direct observation of the land and seas with unique spatial characteristics over long periods of time. To varying degrees, the information collected by each sensor is specifically suited for a range of interests associated with monitoring the effects of human activities or of natural land transformations.

A Synthetic Aperture Radar (SAR) is a powerful Earth observation instrument installed on many recent remote sensing satellites. It can acquire images of the Earth during day or night, in all weather and through cloud cover. Users from the scientific community, military, governmental or any commercial organisations have access to valuable information in such varied fields as agriculture, cartography, hydrology, forestry, oceanography and ice studies [1]. The benefits of this type of technology extend to disaster management and coastal monitoring. Figure 1-1 shows images taken before and after the tsunami disaster in December 2004 of the Sri Lanka's coast line helping in relief efforts by illustrating the differences in landscape.

A new technology is being looked at closely to reduce mass and cost for next generation of SAR antennas. This latest approach consists of using a very lightweight thin sheet of material acting as the emitting surface of the antenna. Having a membrane antenna would allow remote sensing missions to cut cost and weight by a non-negligible factor. New materials and manufacturing technologies have allowed the possibility of building such new antennas.

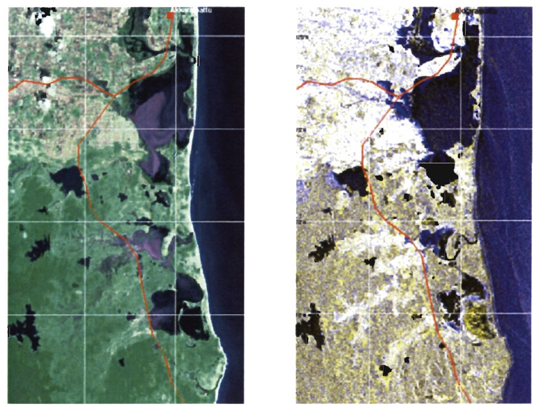

Before **After**

Figure 1-1: SAR images used for the relief efforts of the tsunami in Sri Lanka on 12/26/2004 [2]

These thin membrane structures are subjected to unique operational problems not occurring in conventional antenna structures. Wrinkles, in every day products, are not often critical, but for a planar electrical antenna on a space based radar they can undermine the antenna performance by a significant margin. The functionality of the radar elements on the membrane layer is function of their orientation toward Earth. With conventional metal or composite structures of satellite antennas, the wrinkling phenomena are, of course, not considered as one of the design criteria. However, results from a wrinkling analysis are an important factor that will likely be included within the design process for membrane antennas.

One of the harsh realities of space environment is the wide range of temperatures the satellite is subjected to, depending on whether it is exposed to solar radiations or not, which can create thermally induced wrinkles. It is therefore important to understand the impact of this operational environment on any hardware sent to space.

1.1 Description of the Membrane Antenna

A full antenna design consists of an assembly of three different membrane layers as shown in Figure 1-2, each with its own function and properties. The top layer is called the Radiating Plane with the radiating features. Their orientation toward Earth is subjected to strict tolerances. The radiating elements are regrouped on the surface of this layer in a rectangular area called the electrical aperture. The second and middle layer is called the Ground Plane. For electrical purposes, its surface is entirely covered by chemically deposited copper. The last layer is called the Feed Network Plane. It has chemically deposited copper over a predetermined pattern. The percentage of the area covered depends on the electrical function of the antenna determined by requirements outside the scope of this thesis. The percentage of uncovered area is randomly dispersed from a mechanical point of view.

A cable passes along the parabolic shaped sides. The cable's axial load stretches each membrane layer by creating a uniform in-plane pressure, or tension, throughout the layer. A common example of similar use can be found in any cable-suspended bridge or cable-suspended roof. Figure 1-3 illustrates the three membrane layers as well as the cable tensioning system transmitting the load on both adjacent edges. A constant-load spring (not shown) is located at the connection with the support structure.

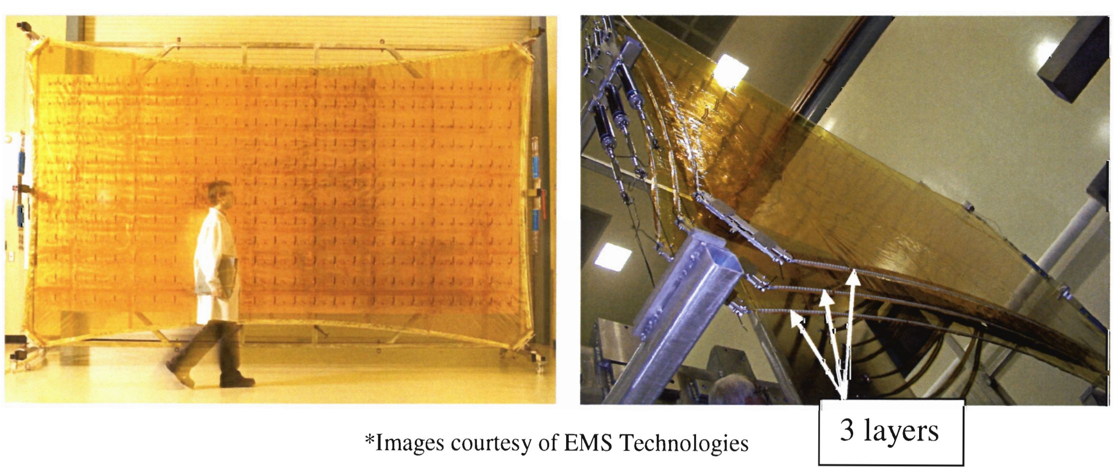

*Images courtesy of EMS Technologies

Figure 1-2 : Pictures of the 2.25 m x 5 m prototype

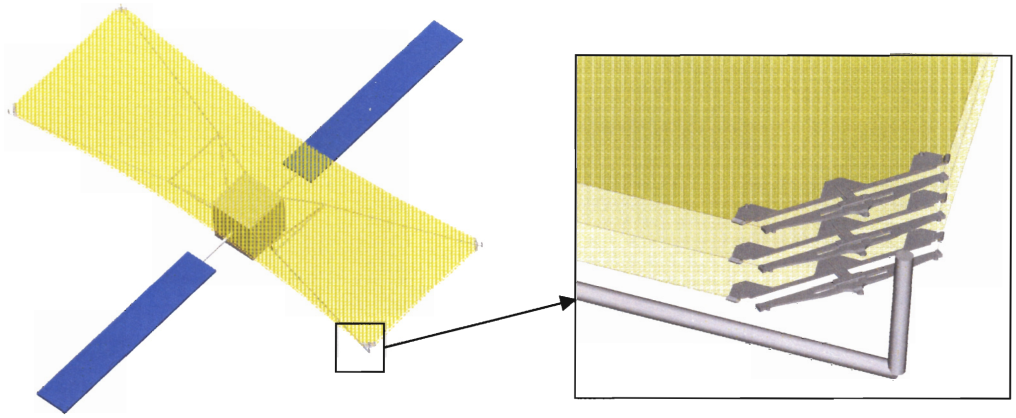

Figure 1-3 : 2.25 m x 10 m membrane design

The antenna life cycle would include folding in a predetermined pattern into a storage compartment, launching and then deploying it in orbit. Understanding the life-cycle of the antenna becomes important for the redesign of the tensioning mechanism undertaken in this thesis.

Independently of the shape design and the dimensions of the antenna, the membrane electrical functions can require the use of particular wavelengths for the radar. For the mechanical design, each wavelength implies a specific number of equally spaced radiating elements on the Radiating Plane. This project studies the proposed L-Band and C-Band wavelength configurations in the dynamic analyses. The complete details and explanation of the difference of both wavelength configurations is irrelevant to this thesis since it concerns electrical aspects. From the mechanical point of view, the main difference is the L-Band configuration has the radiating elements distributed with a spacing of 93.75 mm while the C-Band configuration has an element spacing of 22.1 mm for the same electrical aperture dimensions. Therefore, the latter configuration has many times the number of radiating elements of the L-Band for the same electrical aperture area.

1.2 Literature Review

Study of the wrinkling of membranes is not new. Wagner [3] first introduced in 1929 the tension field theory (TFT), which describes the state of stresses in a membrane when its boundaries are stretched and displaced. This theory has been developed from the observation of a thin-walled web carrying loads several times above the initial buckling value. Reissner [4], in 1938, simplified the lengthy geometrical considerations of this theory. Mansfield [5] extended the TFT to the study of membrane with different shapes and boundary conditions subjected to shear as well as with different material properties.

Stein and Hedgepeth [6] further developed the tension field theory into the theory generally known as wrinkling theory to handle partly wrinkled membranes and more general problems. They made it possible to solve situations in which the stress lines are not parallel. They introduced the principle that membrane cannot carry compressive stresses. The minor principal stress is therefore non-negative in all the membrane. They also explicitly detailed the membrane state as either wrinkled or taut, and explained their condition. The idea that the wrinkles are aligned with the major principal stress direction has allowed them to further develop the theory. They also considered the effects of wrinkling by using a variable Poisson's ratio in the direction of the minor principal stress.

Miller and Hedgepeth [7] adapted the theory in 1982 to the finite element method for analysis of partially wrinkled membranes. Their iterative membrane properties (IMP) method based on the Stein and Hedgepeth theory of wrinkling, uses geometrically non-linear analysis. The method modifies the properties of the elements of the membrane to eliminate the compressive stresses present until only non-negative stresses are left in the membrane. The IMP method cannot predict the height or the orientation of the wrinkles. Only the area affected by wrinkles is known. Adler [8] implemented the IMP finite element solution into the ABAQUS software in 2000.

In 2002, Wong and Pellegrino [9][10][11][12] used the idea of implementing imperfections into the planarity of the membrane to induce out-of-plane bending with compressive stresses. Prior buckling analysis modes of the model determine the initial planarity imperfection distribution on the membrane nodes. The pattern, height and orientation of wrinkles can be predicted with accuracy. Tessler and Sleight [13] showed a similar method using random imperfection distribution with acurate results.

The membrane antenna with predetermined side shapes and in-plane tension could have wrinkles occurring anywhere on its surface. However without knowing the height of these possible wrinkles, it would be impossible to know if they would be within the planarity tolerance. Without knowing the wrinkle height, as would be the case using the IMP method, a valid membrane design with wrinkles within the tolerance limit would have to be started all over again, a costly process. The wrinkle height must be predicted with accuracy. Therefore, this thesis uses the approach followed by Tessler and Sleight for all wrinkling analyses.

1.3 Scope of the Thesis

This thesis focuses on a novel type of Synthetic Aperture Radar (SAR) satellite antenna. A thin membrane layer replaces the conventional composite structure for orienting the radiating features toward Earth.

The membrane layer reduces most of the unnecessary mass of the satellite antenna. The role of the conventional composite structure is only to support statically and dynamically its own weight. The composite structure's mass is not directly related in any manner to the electrical functions of the antenna. Therefore, this mass can and should be removed.

The use of membrane antennas reduces weight and launching cost by a non-negligible factor. New materials and manufacturing technologies have allowed the possibility of building such new antennas. Cables attached on all four edges of the nearly rectangular antenna distribute evenly an in-plane tension stretching the layer. The four sides follow a parabolic shape.

The shape and size of the membrane antenna is determined by many parameters. The cables stretching the membrane require parabolic side shapes to convert into uniform in-plane tension. The variation of the cable axial load and the in-plane tension influences differently the shape and size of the membrane. A study is required to show the impact of the variation of these two parameters on the shape of the membrane. This will help in determining the optimum size and shape of the membrane.

Such an engineering project requires, before launching the first model into orbit, analysis of all possible electrical or mechanical failure modes. With the membrane antennas, a unique type of mechanical failure mode must be looked at: wrinkles. The wrinkling of the radiating layer could greatly undermine the performance of the antenna by rendering the wrinkle-affected area useless. Wrinkles change the orientation of the radiating elements in the affected area. With a SAR, as well as any other type of antenna, orientation is critical. It has been anticipated that such wrinkling could occur with temperature variations in space.

The membrane antenna concept is advantageous by using lighter material and by having a lower launch cost, but there is presently a lack of available analyses for predicting with confidence the behaviour of such stretched structures in space environment. Being such a thin film, the membrane sheet does not support compressive stress as more common structures do. Literature on the subject is much fewer compared to the standard types of satellite structural analyses. Therefore, manufacturers do not have sufficient knowledge to understand and fully predict the behaviour of this promising type of antennas under all conditions.

Space environment involves high thermal gradients. The implications of these thermal gradients on wrinkle formation on the membrane layers have to be known. Preliminary finite element analyses of the membrane designs have shown a uniform stress field at room temperature with a high stress gradient near the corners. Since the corners are already submitted to a non-uniform stress field, the space temperature conditions are expected to favour local wrinkling at these corners.

Accurate prediction of thermally induced wrinkles results in the ability of developing wrinkle control features. These wrinkle control features would allow a better use of the available membrane area and a better optimisation of the design.

The thesis concentrates on predicting the appearance of wrinkles induced by thermal variations and on the feasibility of controlling these wrinkles avoiding loss of flatness of the electrical aperture. This study exploits recent developments in finite element analysis for predicting the height and orientation of wrinkles. The wrinkles looked at are due to localized buckling by compressive stresses and not from permanent creases due to packaging or manufacturing imperfections.

Because of its large size required and its low bending stiffness, the membrane is sensitive to amplification of on-orbit vibrations. The dynamic analyses focus on the membrane response to on-orbit operational micro-vibrations.

1.4 Organization of the Thesis

The thesis has been divided into nine chapters including this introduction. **Chapter 2** lists all data specified and determined by outside sources prior to the start of the work done and presented within this thesis. **Chapter 3** brings to light the impact of different parameters acting on the antenna shape and size and the required tensioning cable loads.

Chapter 4 describes the efforts put in to develop a finite element model to predict wrinkle occurrence as well as the results obtained regarding their height and orientation.

This is the first step for proceeding to further work in the thesis. **Chapter 5** discusses the results obtained by finite element analyses on wrinkles induced by temperature variations. The full and partial exposures of the antenna to solar radiation are explored. This work represents the stepping-stone for the possibility of controlling wrinkles. **Chapter 6** shows the feasibility of controlling wrinkles formed by thermal variations using a passive method. Three designs are presented.

Chapter 7 focuses on the dynamic analysis of such flexible and large structure and on its response to on-orbit micro-vibrations. **Chapter 8** contains the stress analysis of the redesign of the tensioning system for a proposed future prototype.

Chapter 9 presents the conclusion of the thesis with a summary of the work and findings as well as suggestions for future work.

2 DESIGN CONSTRAINTS

Since this project builds on existing and available antenna designs, many parameters and constraints are determined by factors outside the scope of this thesis. For the purpose of consistency with these external sources, the same parametric values are used in this thesis.

2.1 Material

Different materials are used in different finite element models in this thesis. The choices of the materials for the models are determined by the need for consistency with external sources or for consistency throughout this thesis. Table 2-1 describes the important properties of various materials and the corresponding finite element model in which they are used.

In some models, copper chemically deposited over the total or partial area covers the material sheets of two of the three layers of the antenna. When copper fully covers a layer surface, this characteristic can be adequately incorporated in the model. However, for copper covering a partial area of a layer such as for the Feed Network Plane, some software issues should be looked at. The software used can only consider a uniform deposit. Therefore an adequate option of modifying the copper properties according to the percentage of area covered is implemented. More specifically, the copper's modulus of elasticity is multiplied by the same percentage of copper covered area. For example, the Feed Network Plane of the L-Band antenna configuration has 75 % of its area covered by copper. The Young's modulus is therefore multiplied by 0.75 for that specific configuration. Table 2-2 and 2-3 detail the copper characteristics of each layer for L-Band and C-Band configurations taken from various sources as indicated.

Material	**Young's Modulus E** [N/mm^2]	**Poisson Ratio υ**	**Coefficient of Thermal Expansion α** [mm/mm°C]	**Thermal Conductivity** [W/mm-K]	**Density ρ** [kg/mm^3]	**Thickness Used** [mm]	**Model***
Mylar® Polyester Film [13]	3790	0.38	N/A	N/A	N/A	0.0762	SS
Polyimide 1 Film [13]	2590	0.34	0.000015	0.00012	N/A	0.0254	ST, R
Polyimide 2 Film [14]	5377.91	0.32	As per Figure 2-1	0.00012	N/A	0.0254	2.25x5
Aluminium [15]	71 700	0.33	2.36×10^{-5}	0.121	2.81×10^{-6}	1.5875	2.25x5
Polyimide 3 [16]	4826.33	0.32	N/A	N/A	1.52×10^{-7}	0.0504	2.25x10
Copper [15]	110 000	0.34	N/A	N/A	8.96×10^{-6}	.009	2.25x10L
						.0045	2.25x10C
Copper (Reduced Properties)	82 500	0.34	N/A	N/A	8.96×10^{-6}	.009	2.25x10L
	99 000					.0045	2.25x10C
Kevlar® [17]	117 211	0.30	N/A	N/A	1.44×10^{-5}	(Area 1.70 mm^2)	2.25x5 2.25x10

* SS = Square model with shear loads, ST = Square model with tensile loads, R = Rectangular models, 2.25x5 = All 2.25 m x 5 m models, 2.25x10 = All 2.25 m x 10 m models, 2.25x10C = 2.25 m x 10 m C-Band model only, 2.25x10L = 2.25 m x 10 m L-Band model only.

Table 2-1 : Material characteristics

Layer	Thickness [mm]	Copper Coated Area	Copper Thickness [mm]
Radiating Plane	0.0504	0 %	0.000
Ground Plane	0.0504	100 %	0.009
Feed Network Plane	0.0504	75 %	0.009

Table 2-2 : L-Band membrane layers copper composition [17] for the 2.25 m x 10 m model

Layer	Thickness [mm]	Copper Coated Area	Copper Thickness [mm]
Radiating Plane	0.0504	0 %	0.000
Ground Plane	0.0504	100 %	0.0045
Feed Network Plane	0.0504	90 %	0.0045

Table 2-3 : C-Band membrane layers copper composition [17] for the 2.25 m x 10 m model

An external organisation subjected the polyimide 2 material (see Table 2-1) to thermal tests in order to determine the exact value of the temperature dependent CTE [18]. The data available from the manufacturer was found by that organisation to lack precision and without temperature dependent information. Only a single value is supplied [14]. The following results, Figure 2-1 and Table 2-4, were obtained and supplied by that external organisation for implementation into the relevant numerical analyses.

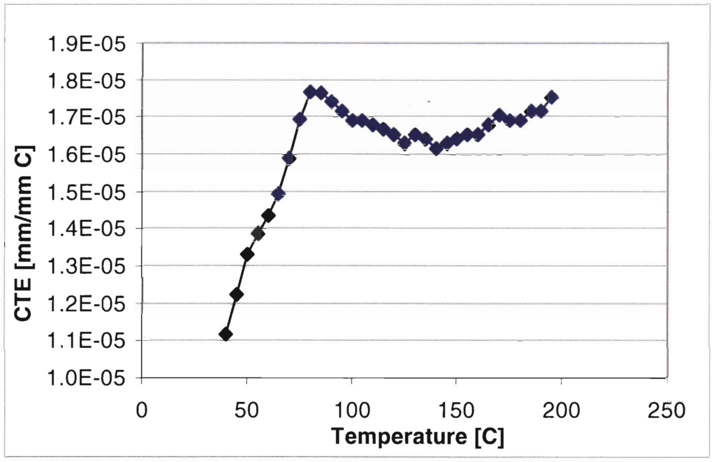

Figure 2-1 : Coefficient of thermal expansion of the polyimide 2 material as determined by experimental tests [18]

Temperature [°C]	Coefficient of Thermal Expansion [x10^{-5} mm/mm°C]	Temperature [°C]	Coefficient of Thermal Expansion [x10^{-5} mm/mm°C]
40	1.1195	120	1.6531
45	1.2261	125	1.6281
50	1.3311	130	1.6531
55	1.3851	135	1.6406
60	1.4352	140	1.6156
65	1.4941	145	1.6281
70	1.5880	150	1.6406
75	1.6920	155	1.6531
80	1.7671	160	1.6531
85	1.7658	165	1.6782
90	1.7408	170	1.7032
95	1.7157	175	1.6907
100	1.6907	180	1.6907
105	1.6907	185	1.7157
110	1.6782	190	1.7157
115	1.6657	195	1.7533

Table 2-4 : Coefficient of thermal expansion of the polyimide 2 material as determined by experimental tests [18]

2.2 2.25 m x 5 m and 2.25 m x 10 m Membrane Designs

An existing 2.25 m x 5 m membrane prototype as shown previously in Figure 1-2, has been used as example for a number of analyses. Materials, dimensions, membrane tensions and many characteristics are used as measured or given. The 2.25 m x 10 m membrane dimensions have not been measured from a physical prototype but extracted from a proposed design still on drawing boards at the time of writing this thesis.

As explained further in section 3.2.1, the equations describing the parabolic shape of the membrane sides need a number of variables describing physical aspects or dimensions. Many of these variables are determined independently by external sources and passed on to this project. Their values are shown in Table 2-5 and 2-6 for both model designs.

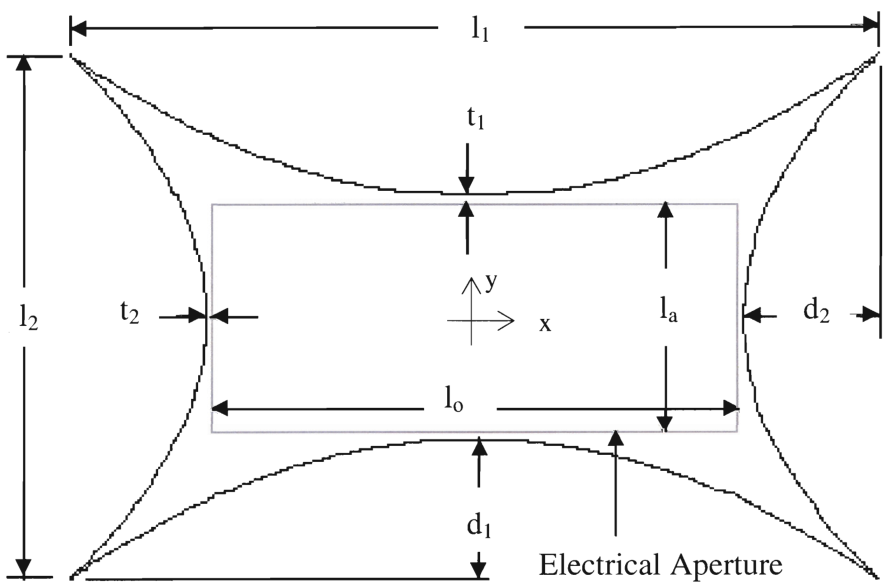

Figure 2-2 : Parameters used in membrane calculations

Figure 2-2 illustrates the rectangular central area called the electrical aperture regrouping all radiating elements of the radar. It should be noted that further along in this thesis, the corners of the membrane will be cut modifying its overall shape.

Description	Variable	Value
Electrical Aperture Length	l_o	4.59 m
Electrical Aperture Width	l_a	2.25 m
Spacing between the Aperture and the Long Side Edge	t_1	93.75 mm
Spacing between the Aperture and the Short Side Edge	t_2	46.89 mm
Corner Edge Length (not shown in Figure 2-2)	e	10 in [254 mm]
Parabolic Parameter ($y=Ax^2$)	A	0.04921 m^{-1}
Parabolic Parameter ($x=Cy^2$)	C	0.04835 m^{-1}
Spacing between Layers	---	2 in [50.8mm]
Layer Thickness	t	0.001 in [0.0254 mm]

Table 2-5 : 2.25 m x 5 m antenna known characteristics [17]

Description	Variable	Value
Electrical Aperture Length	l_o	10 m
Electrical Aperture Width	l_a	2.25 m
Spacing between the Aperture and the Long Side Edge	t_1	93.75 mm
Spacing between the Aperture and the Short Side Edge	t_2	46.89 mm
Corner Edge Length (not shown in Figure 2-2)	e	10 in [254 mm]
Spacing between Layers	---	2 in [50.8mm]
Layer Thickness	t	0.001 in [0.0254 mm]

Table 2-6 : 2.25 m x 10 m antenna known characteristics [17]

2.3 Cable Loads and Membrane In-Plane Tension

One of the initial requirements of the membrane design is for the cable to have the same axial load for all four parabolic sides.

Model	Cable Axial Load [N]	Layer In-Plane Tension [psi (N/m^2)] Axis 1	Layer In-Plane Tension [psi (N/m^2)] Axis 2
2.25 m x 5 m	44.48	25 (172.37)	25 (172.37)
2.25 m x 10 m	355.85	50 (344.74)	50 (344.74)

Table 2-7 : Cable axial load and layer tension [17]

2.4 Temperature Range

Space environment implies rapid and large temperature variations from exposure or non-exposure to solar radiations. Sunshields reduce the importance of these variations depending on their design. Temperature data relating to the orbital exposure of a 2.25 m x 5 m antenna are available from a previous study [19]. Considering different lower and upper sunshields, and different material composition of the various layers of the full antenna, the following table is obtained [19]. The overall maximum and minimum temperatures are taken as operating limits for all thermal analyses. The minimum temperature of -36.1°C is rounded to -40°C [17].

Layer	Maximum Temperature [°C]	Minimum Temperature [°C]
Radiating Plane	11.9	-36.1
Ground Plane	18.8	-33.2
Feed Network Plane	23.4	-31.7

Table 2-8 : Temperature of the antenna layers [19]

The room temperature of the manufacturing and assembly processes for the models is estimated at 20°C, representing the initial models temperature. Any other temperature is a variation from this initial state.

2.5 Antenna Deflection Tolerances

The electrical performance of the antenna is dependent on the planarity of the membrane. The out-of-plane deformation tolerance varies with the wavelength configuration used by the antenna. An L-Band antenna has an allowable deflection of approximately 10 mm [19]. Since a C-Band wavelength is approximately 4 times smaller, the deflection tolerance will also be 4 times smaller at 2.5 mm.

Wavelength Configuration	Allowed Out-of-Plane Displacement [mm]
L-Band Antenna	10.0
C-Band Antenna	2.5

Table 2-9 : Electrical aperture planarity tolerance [19]

These maximum deflections represent a total displacement tolerance that includes manufacturing and assembly errors and misalignment of the support structure. Since the analysis of a support structure is not a part of this thesis, it will be assumed to have perfect planarity.

2.6 On-Orbit Micro-Vibrations

The electrical performance of the antenna requires the electrical aperture out-of-plane displacement to stay within the flatness tolerance mentioned in section 2.5 for all layers. This deflection includes any dynamic response to orbital and operational activities. Levels of expected on-orbit micro-vibrations are shown in Table 2-10.

Frequency Range [Hz]	Excitation Level [g]
0.5 to 3	0.01
3 to 100	Decrease based on $1/f^2$

Table 2-10 : On-orbit micro-vibrations excitation levels [19]

It has been determined amid other considerations that the first natural frequency of the antenna should be higher than 2.0 Hz [17][19]. This limit is governed by the attitude control system of the satellite.

3 MEMBRANE SHAPE DETERMINATION

Membranes stretched by cables such as the one studied in this thesis have specific parabolic shapes on each side to uniformly distribute the cable load into a membrane in-plane pressure, or tension.

The parameters describing the parabolic sides determine the size of the membrane antenna as well as directly affect the required cable axial loads. The cables are passing along the membrane edges. The cable axial loads are transmitted to the support structure influencing its necessary stiffness and wall thickness and at the same time its weight. Therefore, the membrane size influences the weight of the support structure through the cable loads. This impact has not been evaluated or quantified in available literature. This thesis presents such a study on the relationship between the membrane size and its consequence on the weight of the support structure. This analysis will help determine an optimum membrane shape and size.

Before this study is presented, the mathematical relations between the geometric properties, the required cable load and desired in-plane tensions are established.

The total membrane area must be kept as small as possible because of manufacturing constraints. The required cable axial load must also be kept as small as possible to transmit the smallest load onto the support structure and keep its weight to a minimum.

The type of support structure for this membrane antenna design is unknown at the time of writing of the thesis. When the decision on the support structure is made, the value of the allowable maximum load transmitted onto the structure would be known. Then an optimum membrane shape design could be carried out.

3.1 Assumptions for Membrane Shape Design

Three assumptions are made regarding the membrane shape and cable load:

- The parabolic shape of the cable remains unchanged when the tensioning load is applied. The design should yield the desired parabolic shape when fully stretched.

- It is assumed that the friction between the cable and the membrane material is negligible.

3.2 Shape of the Membrane Sides

The theoretically correct equations establishing the shape of the sides of the membrane to distribute the cable axial load into a uniform in-plane tension involves hyperbolic sine and cosine functions. There are approximate theories that have been proved useful. When the catenary shape of the sides is shallow enough, the shape is adequately approximated by a parabola [20][21]. This approximation is valid when the ratio of the parabola height, or depth, over its length d/ℓ (see Figure 2-2) is lower than or equal to 0.3. This limit is respected for all shape designs throughout this thesis. This approximation greatly simplifies the calculations without much loss of accuracy.

For a constant rectangular central electrical aperture as shown in Figure 2-2, the parabolas representing the sides determine the total size and surface of the membrane. The parabola equations and cable axial loads determine the resulting in-plane tensions in the membrane layers. The electrical aperture dimensions are determined by electrical requirements [19] which are beyond the scope of this thesis. A shallow parabolic side produces a smaller total area than a significantly pronounced parabola. The choice of the shape is therefore important and tools should be available to understand its implication and interaction with the resulting in-plane tensions.

Each side of the membrane is dependent on the others and cannot be treated separately. Therefore an understanding of the equations and interactions between each side is essential.

3.2.1 Geometric Properties

Since all sides are interrelated, if the shape of one side is changed, in consequence all other sides must also be modified. Hence the relationship between the sides has to be established.

The main goal of the antenna, under consideration, is to accommodate an electrical aperture. The specified electrical aperture dimensions are denoted by l_o and l_a. Cushion lengths t_1 and t_2, respectively, are added to these dimensions as shown in Figure 2-2 for manufacturing purposes. These small lengths are determined from manufacturing experience [17]. A minimum spacing is necessary because the cable has to be physically attached to the membrane along the parabolic edges using an undisclosed method which requires a minimum gap. If these cushion zones were to be absent from the design, the cable would be directly on the edge of the electrical aperture. The unknown but necessary fixing method would then undoubtedly overstep on the electrical aperture surface. Therefore, the initial rectangular dimensions are $(l_o + t_2)$ x $(l_a + t_1)$.

The parameters l_o, l_a, t_1, t_2, l_1, l_2, d_1 and d_2, shown in Figure 2-2, represent all required parameters to fully describe the complete geometry of the membrane. The design is fully symmetrical about the two in-plane axes. The membrane shape contains two different parabolas. Each parabola describes the shape of two opposite sides. The predetermined ratios d_1/l_1 (parabola depth over length) and d_2/l_2 are used to describe the curved shape of the parabolas assigned to the sides.

The use of these ratios as given parameters at this initial mathematical step is motivated by the possibility they offer to directly and easily modify the parabolic shape as well as the membrane tension and cable load in the resulting equations (as explained later in this chapter). The total length l_1 and width l_2, shown in Figure 2-2, can be expressed as:

$$l_1 = l_o + 2t_2 + 2d_2 \qquad \textbf{3.1}$$

$$l_2 = l_a + 2t_1 + 2d_1 \qquad \textbf{3.2}$$

After some algebraic manipulations, equations 3.1 and 3.2 can be rewritten as:

$$l_1 = \frac{1}{1 - 4\dfrac{d_1}{l_1}\dfrac{d_2}{l_2}}\left(l_o + 2t_2 + 2l_a\frac{d_2}{l_2} + 4\frac{d_2}{l_2}t_1\right) \qquad \textbf{3.3}$$

$$l_2 = \frac{1}{1 - 4\dfrac{d_1}{l_1}\dfrac{d_2}{l_2}}\left(l_a + 2t_1 + 2l_0\frac{d_1}{l_1} + 4\frac{d_1}{l_1}t_2\right) \qquad \textbf{3.4}$$

The l_1 and l_2 parameters have been expressed as functions of l_o, l_a, t_1, t_2, d_1/l_1 and d_2/l_2, all predetermined and known parameters. The ratios d_1/l_1 and d_2/l_2 are not determined by any design constraints. They are initially established as a choice of the curvature of the parabolas. With a coordinate system located at the center of the membrane layer as shown in Figure 2-2, the positions of the four corners, or intersection of the parabolas are given by ($\pm\, l_1/2$, $\pm\, l_2/2$).

3.2.2 Layer Pressure and Cable Load

Aside from the purely geometric factors, other constraints such as the cable load are part of the governing equations of the membrane shape. The relationship between these geometric properties seen so far and the corresponding cable load and membrane in-plane tensions comes from well-documented studies [20][21]. For design purposes (and from requirements outside the scope of this thesis), the cable axial load must be uniform for all sides and the membrane in-plane tensions must be identical for both in-plane directions. Both long (top and bottom) edges have been assigned the subscript 1, and both short (left and right) edges the subscript 2.

The membrane uniform tension has a predetermined value. This tension, or pressure, is expressed in units of force per unit area. The thickness of the layer t must also be initially specified. The existing design of the 2.25 m x 5 m model chosen as an example has both directional in-plane tensions P defined at 25 psi (172.368 kPa) and a membrane thickness of 0.001 in. (0.0000254 m).

The constant-load spring of each corner pulls on two cable ends. The vectors summation is shown in Figure 3-1.

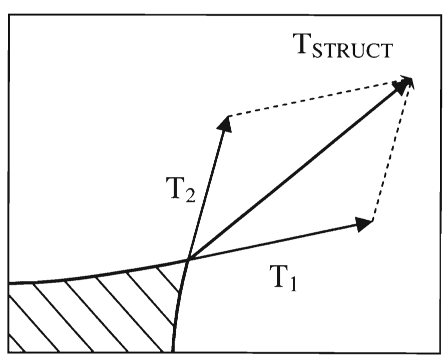

Figure 3-1 : Load vectors and resultant at corners

By design, the cable axial loads, T_1 and T_2, are applied at the end of each parabola. The axial load T is decomposed into its x and y-axis components, H and F/2 respectively, as shown in Figure 3-2 for the top edge. The vectors summation yields the following equation:

$$T_i = \sqrt{H_i^{\ 2} + (F_i/\ 2)^2} \qquad i = 1,2 \qquad \textbf{3.5}$$

The in-plane tension P can be expressed as follows:

$$F_i = Pl_it \qquad i = 1,2 \qquad \textbf{3.6}$$

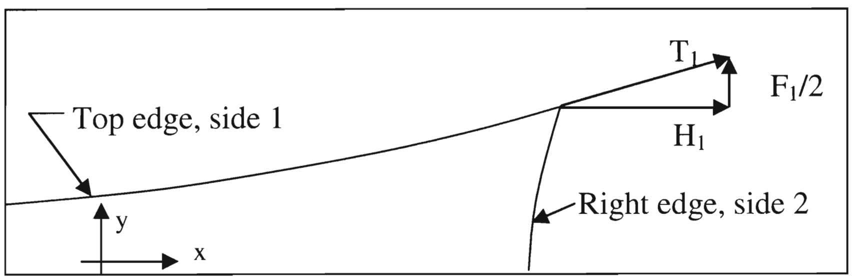

Figure 3-2 : Axial load components decomposition for the top edge

The equations for uniformly distributed loads by parabolic cable are introduced as follows [20]:

$$d_i = \frac{F_i l_i}{8H_i} \qquad i = 1,2 \qquad \textbf{3.7}$$

Combining equations 3.5 and 3.6 with equation 3.7, an expression for the cable load T is obtained. The load is function of the parameters P (tension), l (parabola length), d/ℓ (ratio of parabola depth over length) and t (layer thickness);

$$d_i = \frac{Pl_i^{\ 2}t}{8\sqrt{T_i^{\ 2} - P^2 l_i^{\ 2} t^2 / 4}} \qquad i = 1,2 \qquad \textbf{3.8}$$

or:

$$T_i = \frac{P l_i t}{2}\sqrt{1+\frac{l_i^2}{16 d_i^2}} \qquad i = 1,2 \qquad \textbf{3.9}$$

where

$$T_1 = T_2 = T$$

Equation 3.9 describes how, for a constant and given in-plane tension P, the cable load T decreases with an increase in the parameter d/ℓ. Equation 3.9 is used in the study presented in this chapter.

The difficulty with this approach resides in the initial choice for the values of d_1/l_1 and d_2/l_2 resulting in a cable axial load that is identical for both parabolas, i.e. $T=T_1=T_2$. An iterative process is necessary to adjust the initial choice of these values to obtain a uniform cable load for all sides. This process determines correct d_1/l_1 and d_2/l_2. Only one value has to be iterated or, in other words, only one parabola has to be adjusted in this iterative process.

Another approach is to choose beforehand a desired cable load T then, with these same equations, to find the corresponding parabola equations and geometric characteristics d_1/l_1, d_2/l_2, l_1 and l_2. A set of non-linear equations will then have to be solved to find the geometric characteristics. The choice of the first approach detailed previously is motivated by the ease of an iteration process for engineers over the possibility of solving a set of non-linear equations requiring special mathematical software often not close-at-hand.

For the longer parabolic sides (top and bottom edges), the equation is [20]:

$$y = \frac{F_1}{2H_1 l_1}x^2 + \frac{l_2}{2} - d_1 \qquad \textbf{3.10}$$

and for the shorter sides (left and right edges):

$$x = \frac{F_2}{2H_2 l_2} y^2 + \frac{l_1}{2} - d_2 \qquad \textbf{3.11}$$

It is possible to find the corresponding F_1, F_2, T_1=T_2, d_2/l_2, H_1 and H_2 for a given P, t, d_1/l_1, l_o, l_a, t_1 and t_2 by a simple iteration process using a software such as Microsoft Excel.

3.2.3 Corner Cut-Offs

From the electrical point of view, the area outside the electrical aperture in the corners represents excess and useless material since it does not add to the functionality of the antenna. Depending on the parabolic shapes chosen for the design, the parabolas intersection points can be more or less distant from the membrane center. The further outward these points are, larger is the excess material surface present in the corners as seen in Figure 3-3.

The corners need to be cut to avoid this excess and useless material. Cutting the corners extending outside the electrical aperture reduces the total area. It also directly affects the size and therefore weight of the supporting structure of the membrane antenna. However, the cable load and in-plane tension can remain unchanged. The angle of the resulting corner edge cannot be random. The tensioning mechanism installed along the corner cut-off edge has to pull in the direction of the vector T_{STRUCT} of Figure 3-1. As will be shown later in the thesis, the corner cut-off edge has to be perpendicular to this vector.

Since in the next sections, the impact of modifying the shape of the parabolas is studied, the cutting process has to be defined. Two general methods determining the location of the corners cut are being looked at as shown in Figure 3-3; 1) have a corner cut-off length *e* predetermined, or 2) have a distance *k* from the aperture to the corner cut-off side predetermined. The first method consists of a constant corner cut-off length independent of the shape of the sides. For a pronounced parabolic curve, the corner edge tends to be further out than for a very shallow shape. The second method with a constant distance *k* implies that the length of the corner cut-off is dependent on the curvature of the parabola on each side but always remains at the same distance from the electrical aperture. With the latter method, each modification of the parabolic equation necessitates a tensioning system update.

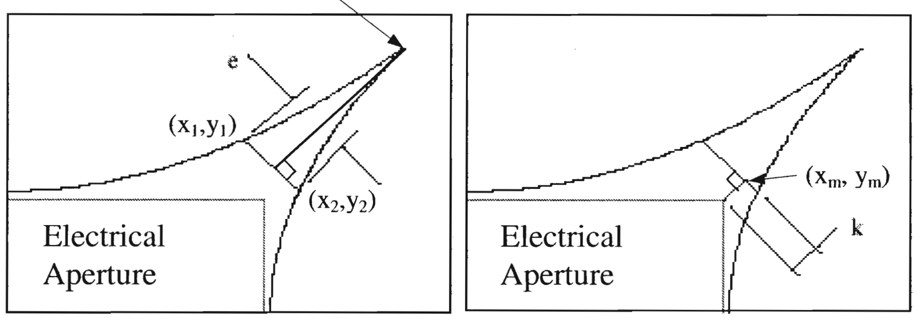

a) Distance *e* constant **b) Distance *k* constant**

Figure 3-3 : Methods used for the corner cut-offs

Both the 2.25 m x 5 m prototype and the proposed 2.25 m x 10 m models use a design with a corner cut-off length *e* fixed at 10 inches (0.254 m). The same tensioning mechanism can therefore be used in either model.

To calculate the position of the two ends of the corner edge (x_1, y_1) and (x_2, y_2) using the method shown in Figure 3-3-(a), a set of four equations with four unknowns (x_1, y_1, x_2, y_2) is solved. The equations are:

$$y_1 = \frac{F_1}{2H_1 \cdot l_1} x_1^2 + \frac{l_2}{2} - d_1 \quad \textbf{3.12}$$

$$x_2 = \frac{F_2}{2H_2 \cdot l_2} y_2^2 + \frac{l_1}{2} - d_2 \quad \textbf{3.13}$$

$$m_e = -\frac{1}{m_{n_e}} = \frac{y_2 - y_1}{x_2 - x_1} = \frac{x_2 + x_1 - l_1}{l_2 - y_2 - y_1} \quad \textbf{3.14}$$

$$e = \sqrt{(y_2 - y_1)^2 + (x_2 - x_1)^2} \qquad \textbf{3.15}$$

Equation 3.14 describes a constraint imposed on the orientation of the corner cut-off as discussed previously. The normal to the corner cut-off edge at its mid-point passes through the intersection point ($l_1/2$, $l_2/2$) of the two parabolas. This intersection point represents, with a negligible error, the correct orientation of the resultant of the cable axial load vectors. This set of equations (3.12 - 3.15) is non-linear and coupled. An iterative solution method is chosen for its efficiency and simplicity. Solving this system analytically proves very cumbersome.

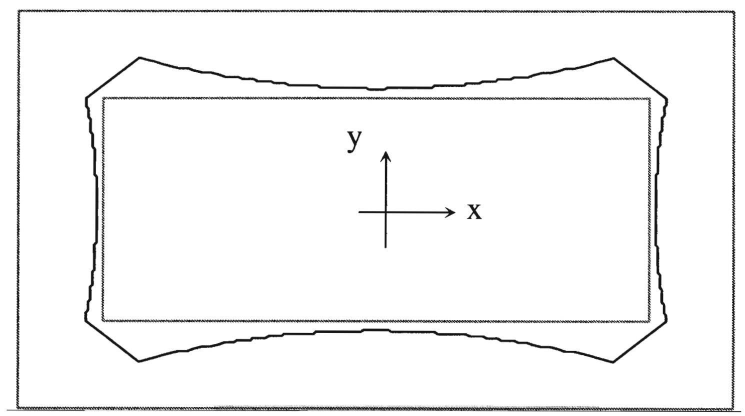

Figure 3-4 : Membrane layer characteristic shape with corners cut

The equations for the case with distance *k* constant are presented in Appendix A.

The value of the total area of the antenna is required for load analysis. Calculation of the total area can be done by more than one method. A geometric method for evaluating the area is chosen by adding and subtracting different subsections specifically chosen for simplifying the calculations. The calculations for the total area with the corner cut-offs are presented in Appendix B.

Since the length and depth of the parabolas have been cut, the cable loads T and the in-plane tensions P have been modified and can be recalculated. However, they were shown to have a negligible difference in all models studied in this thesis. These changes have been estimated to be smaller than the expected manufacturing and assembly errors.

3.3 2.25 m x 5 m Membrane Design

The study presented in this section illustrates the impact of the variation of the membrane total size determined by the parabolic sides on the cable axial load for a constant membrane in-plane tension.

The membrane size is described in this chapter by the ratio of the total area of the layer over the electrical aperture area, or in other words, a ratio representing the area efficiency of the antenna. A ratio closer to 1 results in parabolic curves closer to straight lines almost matching the electrical aperture boundaries. More this ratio increases, more the parabolas are accentuated.

3.3.1 Corner Cut-Offs with Distance *e* Constant

Figure 3-5 represents the impact of the variation of the membrane size, or the change in the parabolic shape, on the required cable load to obtain this shape. As mentioned previously, the membrane size is represented by the ratio of the total membrane area over the electrical aperture area. Equations 3.3, 3.4, and 3.9 - 3.11 are used to calculate the cable axial load. Different in-plane tensions result in different curves.

This plot was obtained for the specified 2.25 m x 5 m electrical aperture dimensions and a corner cut method shown in Figure 3-3-(a) with a length *e* of 0.254 m.

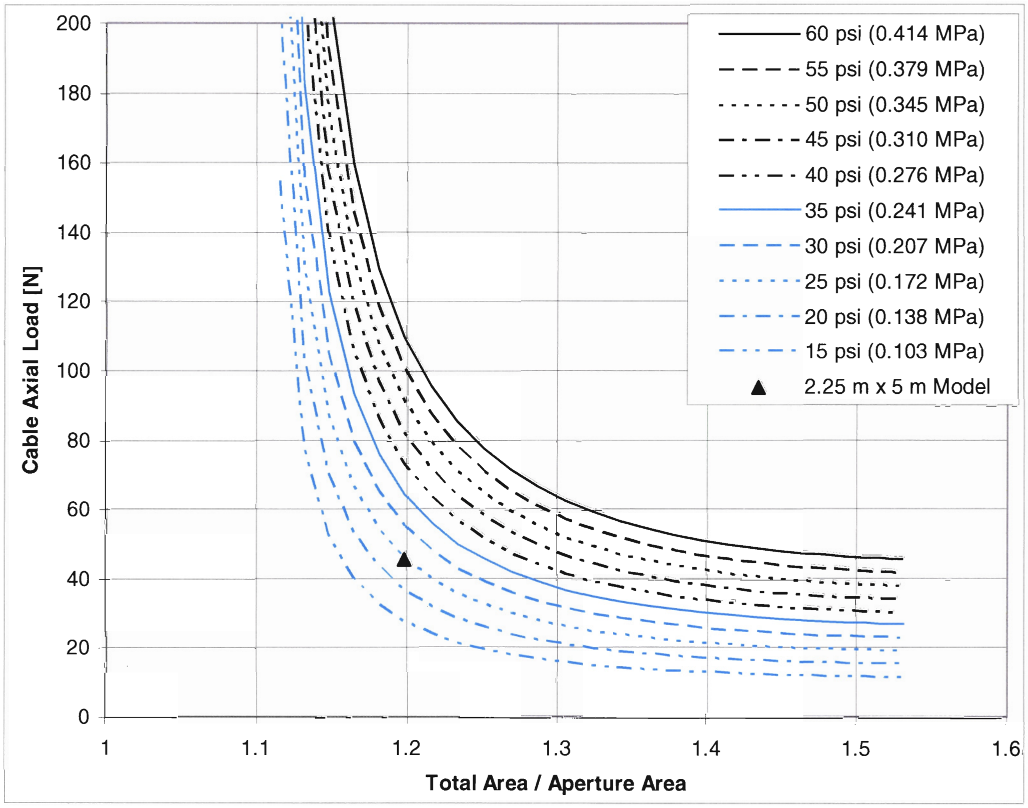

Figure 3-5 : Cable load variation for the 2.25 m x 5 m design with e = 0.254 m

For a smaller area ratio, representing a smaller membrane size where the parabolic side are shallow, the required cable axial load increases. For a larger area ratio, representing a larger membrane where the parabolas are accentuated, the required cable axial load to obtain this shape decreases rapidly but tends to stabilize.

The 2.25 m x 5 m prototype referenced as the baseline for shape, dimensions and comparison point is shown in Figure 3-5 as a triangular mark. The area ratio is approximately 1.2 and the load on the cable to achieve its shape is 44.48 N with a membrane in-plane tension of 25 psi (0.172 MPa). The load transmitted to the structure at the 1.2 ratio level is 74.72 N from the T_1 and T_2 vectors summation as illustrated in Figure 3-1.

To illustrate the use of such analysis as a design tool, an example of possible design variations is shown in Table 3-1. The use of an area ratio of 1.3 instead of the current 1.2 for the 2.25 m x 5 m model with the same membrane tension of 25 psi (0.172 MPa) results in a decrease in the cable load and the load transmitted to the structure. The cable load falls to 26.65 N and the transmitted load to 48.66 N from their initial 44.48 N and 74.72 N respectively. In other words for an increase, for this example, of 8.40 % of the total area of the membrane, the cable load decreases by 40.03 % and the transmitted load to the support structure reduces by 34.88 %.

The decrease in the cable axial load is not the same as that for the transmitted load to the support structure, because the modification of the parabolic shape of the side also modifies the summation of the cable axial load vectors.

Ratio of Total / Aperture Areas	Cable Axial Load	Load on Support Structure	Area Variation	Cable Axial Load Variation	Load Variation on Support Structure
1.2	44.48 N	74.72 N			
1.3	26.65 N	48.66 N	+ 8.40 %	- 40.03 %	- 34.88 %

Table 3-1 : 2.25 m x 5 m model impact of the area ratio variation using e=0.254m

As seen in the results of Table 3-1, the increase to an area ratio of 1.3 from the current prototype ratio of 1.2 would increase its size. Consequently, it would also increase the size of the support structure and inevitably its weight. On the other hand, Table 3-1 also shows that the necessary stiffness of that support structure decreases since the load also decreases which reduces its necessary wall thickness and consequently its weight. The same example of increasing the area ratio of the membrane has the consequence of both increasing and decreasing the weight of the support structure but in different proportions. Since the type of support structure is not known, it is not possible to evaluate and quantify the impact on the weight of the support structure.

3.3.2 Corner Cut-Offs with Distance *k* Constant

Figure 3-6 shows the results of an analysis with the same aperture dimensions as the previous figure, except that it uses method b) of Figure 3-3 by specifying a distance k=0.209 m between the electrical aperture and the corner. This distance applies to the 2.25 m x 5 m prototype.

The curves in the graph of Figure 3-6 end before the ratio reaches 1.35 since the d/ℓ ratio, describing the parabolic shape of the edges, mathematically becomes larger than 0.3 for the long edges (the top and bottom sides) of the membrane. The parabolic assumption for the shape of the sides is valid for a d/ℓ ratio lower than 0.3 as discussed previously.

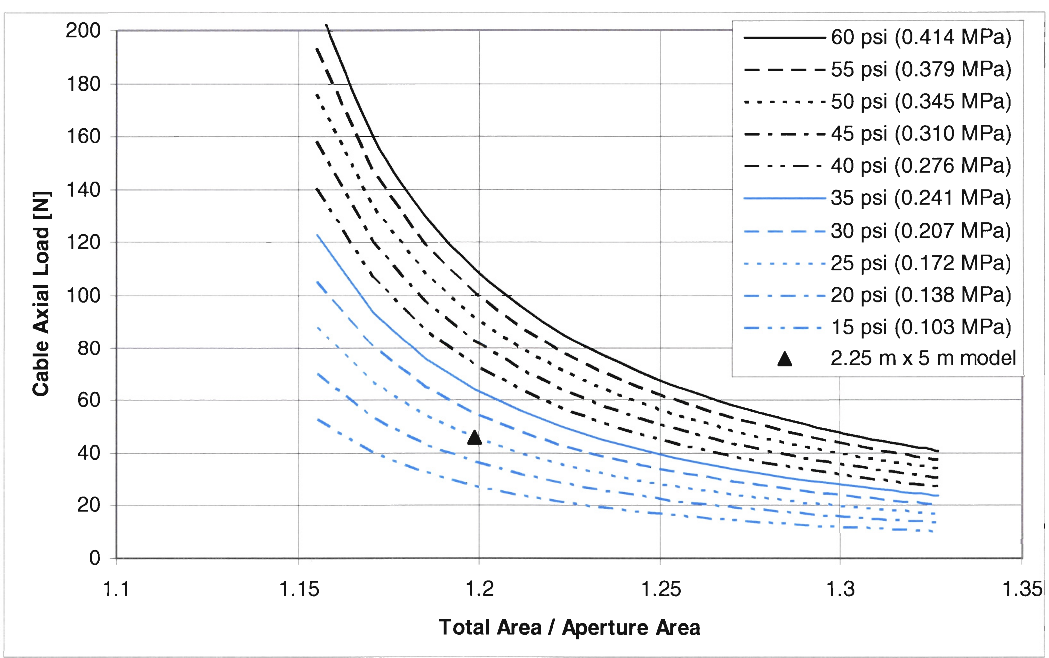

Figure 3-6 : Cable load variation for the 2.25 m x 5 m design with k = 0.209 m

Ratio of Total / Aperture Areas	Cable Axial Load	Load on Support Structure	Area Variation	Cable Axial Load Variation	Load Variation on Support Structure
1.2	44.48 N	74.72 N			
1.3	19.92 N	40.02 N	+ 8.40 %	- 55.19 %	- 46.44 %

Table 3-2 : 2.25 m x 5 m model impact of the area ratio variation using k=0.209m

The earlier example of the impact of an increase in the area ratio from 1.2 to 1.3 is also considered for this set of results as shown in Table 3-2. An increase of 8.40 % of the total area results in a 55.19 % decrease in the required cable load to keep the membrane in-plane tension at 25 psi (0.172 MPa).

3.4 2.25 m x 10 m Membrane Design

Similar calculations for the 2.25 m x 10 m proposed model are presented in this section.

The proposed 2.25 m x 10 m model represented by markers in both Figure 3-7 and Figure 3-8, has a ratio of the total membrane area over electrical aperture area of 1.18, and a membrane in-plane tension of 50 psi (0.345 MPa) corresponding to a cable axial load of 355.85 N.

3.4.1 Corner Cut-Offs with Distance *e* Constant

Two examples of design variation are shown in Table 3-3. The area ratios in these variations are 1.3 and 1.4, as opposed to 1.18 for the proposed model.

When the area ratio is increased to 1.3, the cable axial load decreases by 51.28 % from 355.85 N to 173.36 N. The surface increases by 9.88 %. The transmitted load to the support structure decreases from 540.37 N to 282.88 N, a reduction of 47.65 %.

An area ratio variation from 1.18 to 1.4 decreases the transmitted load to the support structure by 60.38 % to 214.09 N for an increase in the membrane total area of 17.93 %. The cable axial load decreases by 65.27 % to 123.59 N.

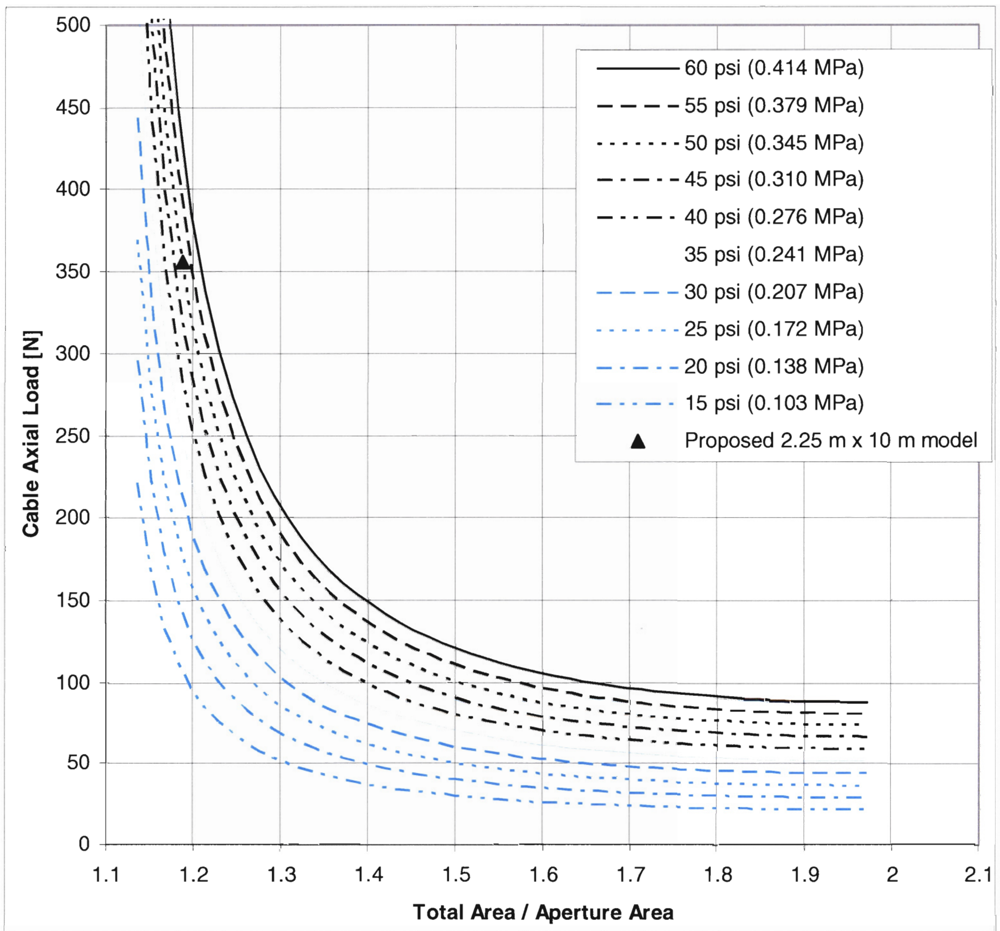

Figure 3-7 : Cable load variation for the 2.25 m x 10 m design with e = 0.254 m

Ratio of Total / Aperture Areas	Cable Axial Load	Load on Support Structure	Area Variation	Cable Axial Load Variation	Load Variation on Support Structure
1.18	355.85 N	540.37 N			
1.3	173.36 N	282.88 N	+ 9.88 %	- 51.28 %	- 47.65 %
1.4	123.59 N	214.09 N	+ 17.93 %	- 65.27 %	- 60.38 %

Table 3-3 : 2.25 m x 10 m model impact of the area ratio variation using e=0.254m

3.4.2 Corner Cut-Offs with Distance *k* Constant

The examples of design variation given in Table 3-4 show for an area ratio change to 1.3, i.e. an area increase of 9.88 %, a decrease of the cable axial load by 58.74 % and the transmitted load to the support structure by 55.07 %. For a modification of the area ratio to 1.4 (the area increases by 17.93 %), the cable axial load and transmitted load decrease to 91.70 N, by 74.23 %, and to 166.18 N, by 69.32 %, respectively.

Ratio of Total / Aperture Areas	Cable Axial Load	Load on Support Structure	Area Variation	Cable Axial Load Variation	Load Variation on Support Structure
1.18	355.85 N	541.60 N			
1.3	146.83 N	243.34 N	+ 9.88 %	- 58.74 %	- 55.07 %
1.4	91.70 N	166.18 N	+ 17.93 %	- 74.23 %	- 69.32 %

Table 3-4 : 2.25 m x 10 m model impact of the area ratio variation using k=0.209m

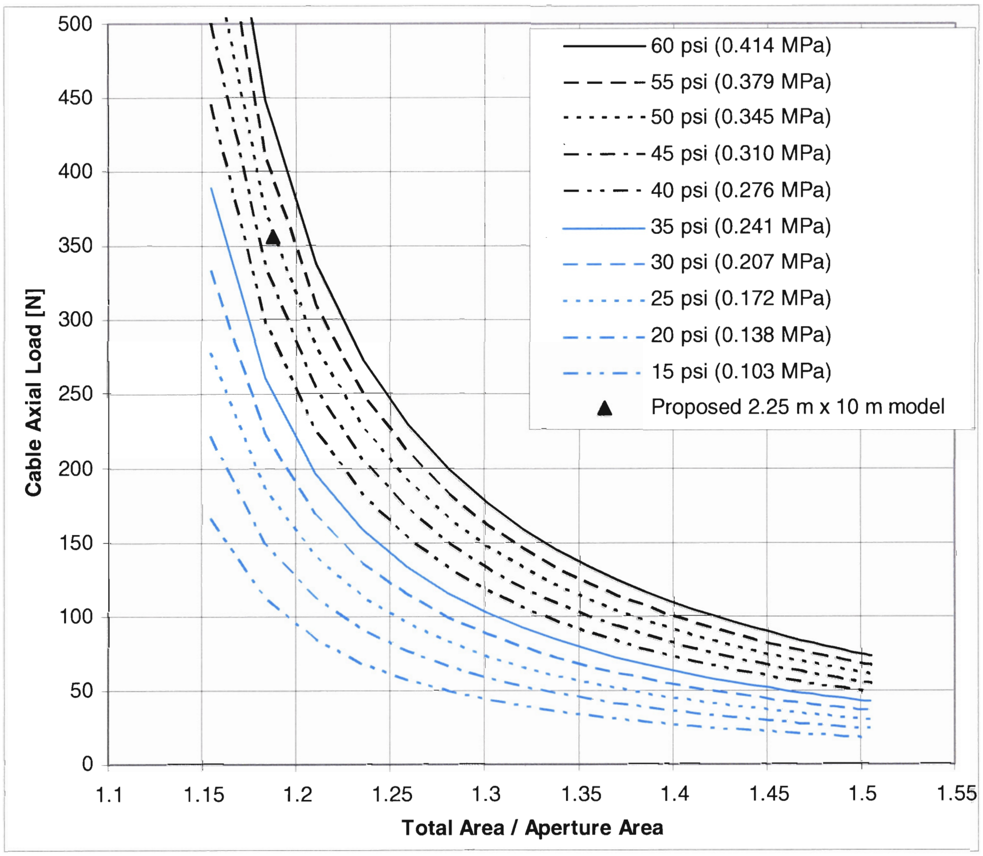

Figure 3-8 : Cable load variation for the 2.25 m x 10 m design with k = 0.209 m

Increasing the membrane area also increases the support structure's size but decreases the required cable axial load. It also results in added difficulty in manufacturing, assembly, folding and deployment. On the other hand, a cable load drop results in a desirable weight diminution by the reduction of the wall thickness of the support structure, smaller cable diameters, smaller tensioning system parts, etc.

The trend on the graphs shows that the cable load decreases rapidly for an increasing ratio closer to 1.0 and tends to level afterwards. Modifying the parabolic shape might result in a considerable decrease in cable load implicating a decrease in the support structure's size and weight. The gains and losses have to be quantified for a possible optimisation, which can only be completed when the type of support structure is known.

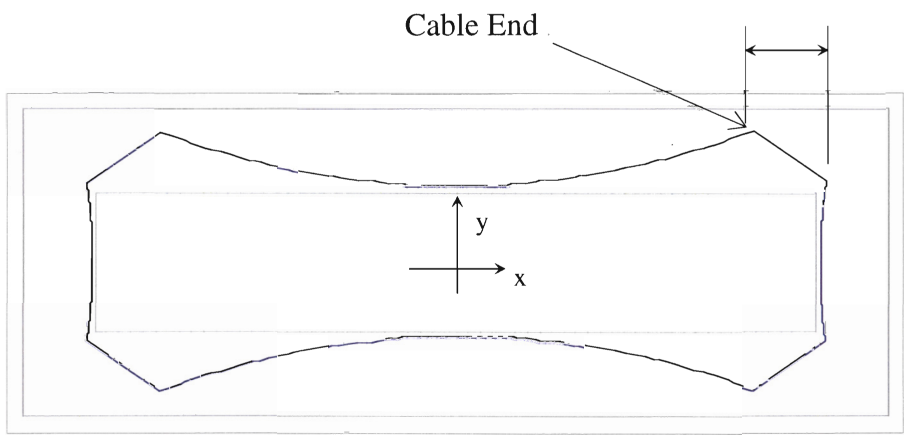

Figure 3-9 : Hypothetical 2.25 m x 10 m model at 50 psi with an area ratio of 1.4

Comparing the results from both methods, it seems preferable to use a calculation and design base on the approach with the corner-to-aperture distance *k* constant. However, this method raises concerns over two issues: first, the resulting length of the tensioning system must match the corner cut-off edge length which could be difficult, and second, the pronounced parabolas could result in important areas without any in-plane tension. Figure 3-9 illustrates such area without any in-plane tension from the top edge parabola. While the other method has a constant corner length of 0.254 m, the example of a possible design shown in Figure 3-9 displays a corner length of 1.295 m.

4 WRINKLING ANALYSIS WITH MECHANICAL LOADS ONLY

Correctly predicting structural behaviour in the space environment is an essential requirement for designing any satellite component.

This project uses a type of material for space antennas not common to commercial satellites and more specifically to Synthetic Aperture Radar (SAR) antennas. In the present case, a polyimide film is stretched into an emitting surface.

While being unquestionably lighter, thus cheaper to launch, there is currently a lack of available analyses for predicting with confidence the behaviour of such stretched material in a space environment especially concerning wrinkle formation. The layer sheets, being thin films, do not support compressive stresses like more common materials such as metal or composite structures. They wrinkle when submitted to compressive stresses.

A need to understand and predict the behaviour of these promising types of antennas has developed with the introduction of such structure into satellite missions. Structural and design engineers have access to very scant literature on the subject. The capability of correctly predicting the location, orientation and height of wrinkles is necessary before investing in the manufacturing of a commercial satellite antenna.

Methods for wrinkling analysis reviewed in chapter 1 modify, in almost every case, the code of the software or add sub-routines, such as the Stein and Hegdepeth IMP approach. They cannot predict the height or the orientation of such wrinkles. Only the area affected by wrinkle is adequately predicted.

An approach to finite elements recently suggested [11][13], demonstrates that FEA models can correctly predict wrinkle height and orientation for models under tension or shear loads. This solution implements initial planarity imperfections in the model. This chapter of the thesis applies this method to more complicated models and, in the next chapter, incorporates thermal loads, which have not or seldom been considered for wrinkle analysis. The use of a commercial software adds to the value of the proposed approach. Since no mathematical modifications or subroutines are necessary, the probability that engineers will adopt it, is enhanced.

Wrinkles are, by definition, large displacements. The finite element analysis software must have the large displacement theory incorporated in its non-linear module. Since the Abaqus software is used in some referenced articles, and since some analysis are reprocessed for comparison in this chapter, all analyses will be conducted using this software for consistency purposes. Considering the popularity of the MSC.Nastran software in structural engineering throughout engineering departments worldwide, results from parallel analyses using this software are also presented. A comparison of results is presented whenever applicable.

Objectives of this thesis include proving the feasibility of controlling the extent, height and orientation of wrinkles induced by thermal variations. To attain this objective, this thesis proposes extending the imperfection approach and proving its stability to more complex geometry, material properties and tensile load cases before demonstrating the feasibility of including thermal loads into the finite element models.

This chapter discusses the development for the models with tensile and shear loads models only.

4.1 Wrinkling Criteria

Detailed discussion of the phenomenon of wrinkling or of any analytical methods to predict wrinkle formation is beyond the scope of this thesis. However, a brief overview of the wrinkling criteria is presented.

There are three different criteria for the onset of wrinkling, namely the principal stresses $\sigma_{1,2}$ criterion, the principal strains $\varepsilon_{1,2}$ criterion and the combined criterion, involving both principal stresses and principal strains.

For the wrinkling criteria based on principal stresses or strains, the membrane is said to be in a *taut* condition when both the principal stresses, or strains, are positive or tensile. The wrinkling occurs in the membrane when the minor principal stress, or strain, is zero and the major principal stress, or strain is in tension.

For wrinkling based on the combined criterion, the membrane is in the *taut* condition when the minor principal stress is positive. The membrane is in a *wrinkled* state, when the maximum principal strain is positive and the minor principal stress is zero (it cannot be compressive).

The wrinkling criteria are summarized below:

<u>Stress criterion</u>

Taut	$\sigma_2 > 0$
Slack	$\sigma_1 \leq 0$
Wrinkled	$\sigma_1 > 0 \ \ \& \ \ \sigma_2 \leq 0$

<u>Strain criterion</u>

Taut	$\varepsilon_1 > 0 \ \ \& \ \ \varepsilon_2 > -\upsilon\varepsilon_1$
Slack	$\varepsilon_1 \leq 0 \ \ \& \ \ \varepsilon_2 \leq 0$
Wrinkled	$\varepsilon_1 > 0 \ \ \& \ \ \varepsilon_2 \leq -\upsilon\varepsilon_1$

<u>Combined stress-strain criterion</u>

Taut	$\sigma_2 > 0$
Slack	$\varepsilon_1 \le 0$
Wrinkled	$\varepsilon_1 > 0$ & $\sigma_2 \le 0$

In the above, σ_1, σ_2 are the principal stresses and ε_1, ε_2 are the principal strains, respectively.

4.2 Assumptions for Wrinkling Analysis

Many assumptions and hypotheses are necessary to reduce the complexity of the numerical models. These assumptions focus mostly on the boundary conditions. They are enumerated without any specific order of importance.

- The parabolic edges of the membrane do not allow out-of-plane displacements, or wrinkles. The cable physically prevents it.

- Gravity is assumed to have no noticeable effect on the experiments and is therefore neglected for all numerical models.

- The studied layers of the membrane are assumed to be composed of polyimide materials only. On the 2.25 m x 5 m prototype, two layers have a thin copper film chemically deposited.

- It is assumed that the manufacturing and assembly of the membrane do not create initial wrinkles.

- The sliding of the cable-membrane interface is considered to be perfect, without friction, preventing any shear to be transmitted to and from the membrane.

- It is assumed that the adhesive tape between each polyimide material sheet composing each layer does not influence the stress field or the wrinkling behaviour in any circumstance.

- The parabolic shape of the cable remains unchanged when the tensioning load is applied. The design should yield the desired parabolic shape when fully stretched.

4.3 Details of the Finite Element Modeling

The information provided in this section also applies to the models and analyses of chapters 5 and 6.

The Abaqus 6.4.1 software provides a new approach capable of predicting the formation of wrinkles with their wavelength and amplitude. All models use the S4R5 element type which has the following characteristics: five nodes shear-deformable shell element incorporating large displacement theory, geometrical non-linear updated Lagrangian theory and small strain assumption. This element also employs reduced integration and an hourglass control method to suppress spurious zero-energy modes. A STABILIZE parameter, provided by the software, is used to add damping to prevent unstable and singular solutions. The value of this parameter should always be kept as low as possible for convergence.

A different approach, modeled on the characteristics enumerated above is applied to the MSC.Nastran 2004 software models. A common 4-node, CQUAD4 shell is used for all elements of the models. A stabilize parameter is included as material damping, which is kept as low as possible for increased accuracy instead of a fictitious viscous damping used with the Abaqus code. No reduced integration method is involved. The shell properties of the element offer the possibility of modifying the bending stiffness of the shell. The bending stiffness is reduced to the smallest value possible for convergence. Reducing the bending stiffness mimics the behaviour of a membrane, which has a very small resistance to bending moments. A value of zero for this bending stiffness parameter would mathematically prevent any coupling in the out-of-plane direction. The K6ROT parameter is set to a value of 1000 accordingly to a previous external study [22].

The proposed method for predicting wrinkle height and orientation uses initial imperfections in the planarity of the membranes to initiate wrinkles [13]. The height of the imperfections is randomly selected within a range of ± 10 % of the thickness of the membrane. The imperfections are distributed over the entire surface (on the nodes) of the membrane except for the edges.

Programs developed in Visual Basic are used to create the nodes and elements for both square models (described in section 4.4.1 and 4.4.2) as well as for the rectangular model (section 4.4.3). These programs are valuable resources for modification of the number of elements but they are not essential for creating the models. The 2.25 m x 5 m model shape is created with the Pro-Engineer 2001 parametric modelling software. Because the Abaqus meshing module lacks the capability of controlling with efficiency the meshing process, the MSC.Patran is used to create the mesh. This MSC.Patran software generates the appropriate input files for both Abaqus and MSC.Nastran to be read and analyzed.

The 2.25 m x 5 m finite element models incorporate an aluminium plate present in the corners as seen in Figure 1-3. The models feature this part because it alters the local behaviour, model stiffness and wrinkle pattern. The hypothetical support structure underneath the membrane shown in Figure 1-3 is not considered since its type and properties are unknown.

The tensioning of the membrane achieved by cables on the prototype is simulated in the numerical analyses by distributed loads creating a uniform and predetermined in-plane tension for both x and y-directions. Since the Abaqus software lacks the capability of applying distributed loads, equivalent concentrated loads are applied on the nodes of the parabolic edges.

Symmetrical characteristics of the membrane are exploited to reduce the size of the models and the computer power and time required for each analysis. Only a quarter of the full 2.25 m x 5 m antenna is modeled whenever possible. Consequent boundary conditions are applied. All displacement results are in millimetres.

4.4 Finite Element Model Results

The work done on wrinkling analyses is discussed in two separate chapters: one for physical loads and the other for the incorporation of thermal loads. This chapter presents the discussions of the results obtained with the finite element analysis with the physical loads.

A rectangular model is created with particular boundary conditions and tensile loads favouring wrinkle formation to which thermal loads are added in the next chapter for comparison. The 2.25 m x 5 m model is analyzed and results are presented. Also, two analyses are reproduced from a previous study [13] to compare results from two different softwares and to validate the finite element models.

4.4.1 Square Model with Shear Loads

The finite element analysis of the square model with shear loads is shown in a referenced article [13] and is compared with experimental results. These numerical and experimental results are reproduced in Figure 4-1. The 229 mm side square piece of Mylar® had all 6 degrees of freedom (DOF) fixed on the bottom edge while the top edge is displaced by 1 mm to the left with all other DOFs restrained.

It is not known if the results in Figure 4-1-(b) take into consideration the effect of gravity on the model, which could explain the difference between the results of two Abaqus analyses.

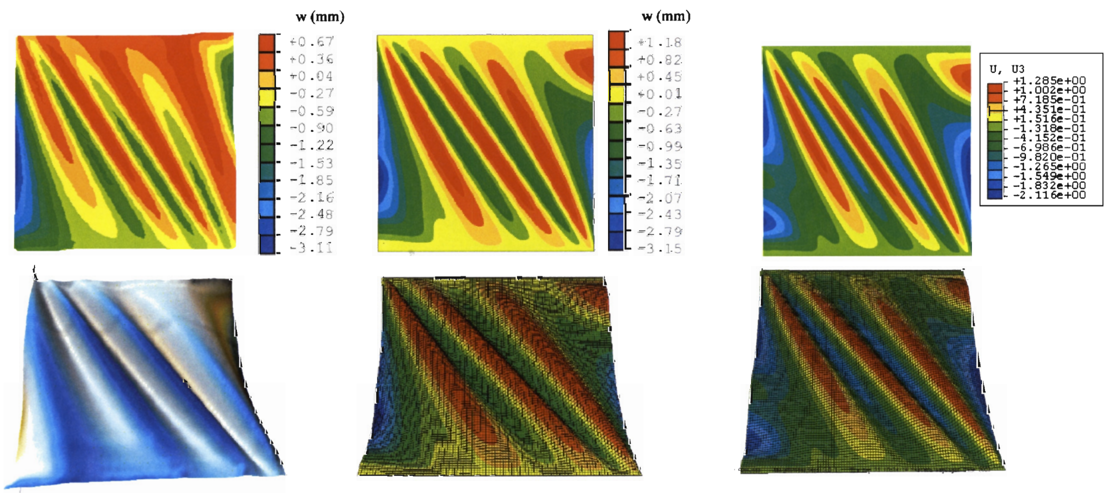

a) Experimental results in [13] **b) Abaqus S4R5 in [13]** **c) Abaqus S4R5**

Figure 4-1 : Wrinkling of a square membrane with shear loads

The MSC.Nastran results illustrated in Figure 4-2 show an accurate correlation with the experimental and the Abaqus results. The MSC.Nastran returned 4 main diagonal wrinkles while the Abaqus results have 3. The experimental results in Figure 4-1-(a) show 4 main diagonal wrinkles. This difference can be explained by separate possible numerical equilibrium solutions for the wrinkle state. The difference in the nature of the damping ratio and its value could also be the reason for the convergence on a different equilibrium state.

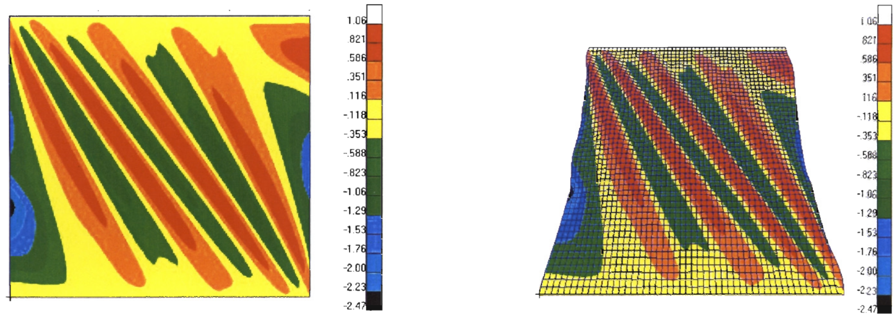

Figure 4-2 : Wrinkling of a square membrane with shear loads using MSC.Nastran CQUAD4 shell elements

The results from the experimental test are satisfactorily reproduced with both Abaqus and MSC.Nastran. These results are all shown to demonstrate the capability of MSC.Nastran to efficiently predict the height and orientation of wrinkles for this model.

In order to establish a complete solution using MSC.Nastran, a study on the impact of the bending stiffness ratio is conducted. This coefficient varies the bending stiffness for a homogeneous shell [23]. The use of a coefficient used in the MSC.Nastran solver proves to be essential in having coupling in the out-of-plane deformation, i.e. wrinkle formation.

From the theoretical point of view, a membrane has no bending stiffness. The bending stiffness coefficient must be as small as possible to represent a membrane. The value of this coefficient was chosen as low as the software will allow it and still converge on a solution. A value of zero leads to divergence and no solution is obtained. Possibly more than one analysis is required, with each having a lower bending stiffness ratio until the software solver diverges.

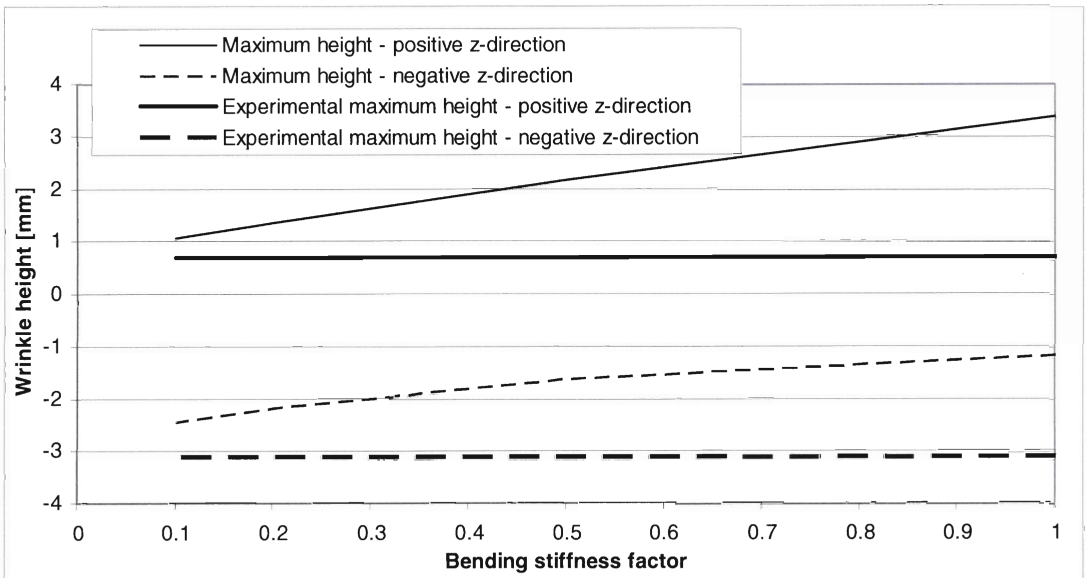

Figure 4-3 : Wrinkle height with respect to bending stiffness value for the square model with shear loads

The bending stiffness parameter in the finite element model is gradually varied to provide an accurate account of the influence of the parameter on the results. Figure 4-3 shows that when the bending stiffness is reduced, the results of the analysis converge to the one from the experimental test.

4.4.2 Square Model with Tensile Loads

This specific analysis consists of reproducing an example shown in [13]. This experiment in [13] studies the wrinkles occurring on a square piece of membrane subjected to opposite tensile loads at each corner. The objective for conducting this analysis is to develop the capabilities for using the imperfection approach and comparing results with an MSC.Nastran analysis.

This analysis represents a closer situation to the stretched SAR membrane antenna than in the previous experiment under shear load. The 2.25 m x 5 m model has only tensile loads and no shear loads.

A 500 mm long square piece of polyimide 1 material (see Table 2-1) is pulled at each corner by a 2.45 N tensile load. The loads are in opposite directions along the two diagonals of the square membrane. In order to prevent a near-singular membrane stress field at the corners and also to prevent the quadrilateral elements collapsing into triangles at the corners (generating high bending stiffness), the corners are cut. The corner cut results in a new edge of 7 mm of length on which the 2.45 N load is modified into an equivalent distributed load.

A problem occurred when the results described in the paper [13] could not be reproduced by following the detailed procedure. The authors were contacted and it was found that the article presented the wrong set of boundary conditions as opposed to the ones used in the actual numerical analysis. The top and bottom corners have the DOFs x, z and θ_y constrained and the left and right corners have the DOFs y, z and θ_x restricted only at the middle node on the corner cut edges. With this new set of boundary conditions applied, the results from both Abaqus and MSC.Nastran analyses are satisfactory. This situation illustrates the importance and sensitivity of the boundary conditions to wrinkling analyses. The incorrect set of conditions prevents wrinkle formation where it should occur.

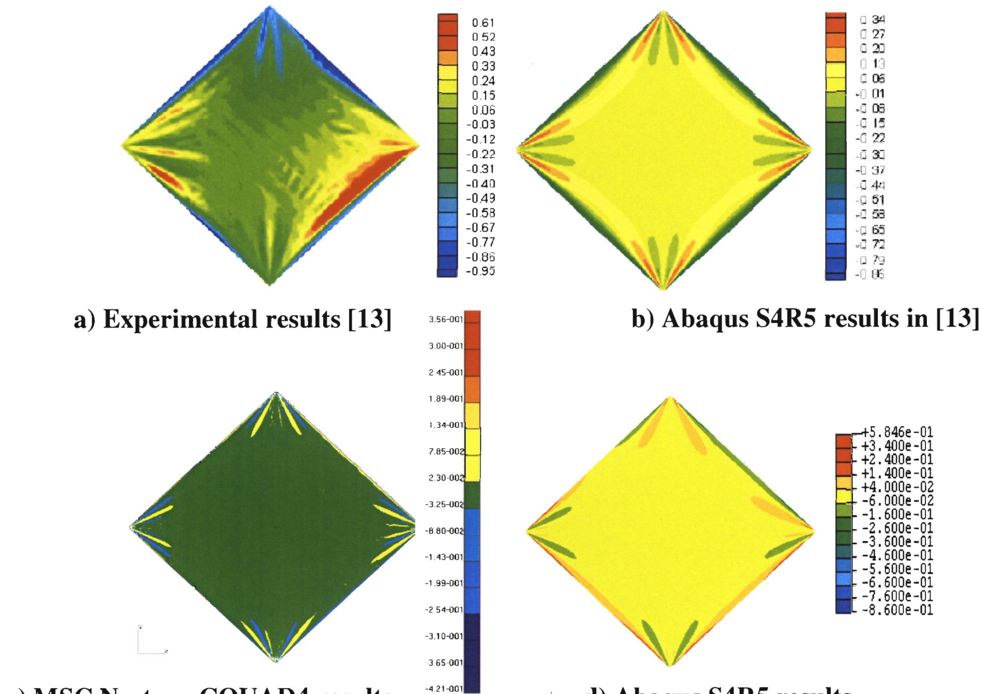

a) Experimental results [13] **b) Abaqus S4R5 results in [13]**

c) MSC.Nastran CQUAD4 results **d) Abaqus S4R5 results**

Figure 4-4 : Wrinkling of a square membrane with tensile loads

The results in the corners show unusual and unexpected local out-of-plane deflections, more specifically on the 7 mm corner cut-offs. Removing the few nodes affected by those local unexpectedly high deformations from the result scale yields the same scale in Figure 4-4-(d) as in Figure 4-4-(b) (both are Abaqus analysis). The result scale in Figure 4-4-(c) and Figure 4-4-(d) are not adjusted to remove those few nodes with unexpectedly high deformation. The full scale of the result has been kept in these illustrations to outline this situation.

The comparison of results obtained shows for physical loads that both Abaqus and MSC.Nastran can be used for wrinkle analysis with tension or shear loads although small discrepancies still exist between the results obtained from the two softwares.

4.4.3 Rectangular Model

The purpose for building and using this rectangular model is to compare results between identical wrinkled models without and with thermal loads. The possibility of extending the random imperfection approach to thermal loads is demonstrated with this comparison. This 300 x 500 mm rectangular model shown in Figure 4-5 is used for comparison. Both heating and cooling cases are studied and presented in the next chapter.

The boundary conditions on the rectangular model as shown below restrict all DOFs of the two corners of the left edge of the model. Only the four nodes on the left edge nearest to both corners have this boundary restriction. The tension loads are applied at 45° angle on the two right edge corners as shown in Figure 4-5. The 2.8 N corner loads are modified into equivalent distributed loads for the 10.6 mm long, 45° angle corner cut-offs. The thickness of the model sheet is 0.001 in. (0.0254 mm). The S4R5 elements are used with a STABILIZE parameter of 0.002.

Figure 4-5 : Rectangular model – Tensile loads – Abaqus S4R5 elements

The out-of-plane displacement pattern obtained from the numerical analysis is consistent with the expected results. The displacement of the left side center area caused by the pulling effect of the right edge tensile loads creates a compressive effect in that same area generating the horizontal wrinkles. Tensile effects create the diagonal winkles from the left edge corners to the membrane center similarly as the square membrane pulled at each of its four corners.

The results obtained from MSC.Nastran using common CQUAD4 elements and a reduction of the bending stiffness parameter to 0.16, are not consistent with the Abaqus results for the height and pattern of the wrinkles. Similarities between the two numerical results include common diagonal wrinkles from the fixed corners toward the model center both in comparable height and number of wrinkles. The wrinkle-affected area located near the center of the left edge has a similar size although the pattern and height of the wrinkles differ for the two result cases. The Abaqus model shows numerous wrinkles with a short wave length compared to the MSC.Nastran results showing fewer wrinkles with increased height. The bending stiffness factor used in MSC.Nastran could offer an explanation. While a lower coefficient provoked a divergence in the solver, this bending stiffness factor could imply an over-stiffening of the model. This over-stiffness resists the compressive effect of that specific region and explains the lesser number of wrinkles present and their increased height compared to the Abaqus results.

Figure 4-6 : Rectangular model – Tensile loads – MSC.Nastran CQUAD4 elements

A simple qualitative physical test with the correct material and shape shows the number of wrinkles to be closer to the Abaqus results than the 4 main diagonal wrinkles and the 3 wrinkles at the left edge predicted by of the MSC.Nastran analysis. The use of the MSC.Nastran software is therefore abandoned.

The number, height and orientation of these wrinkles cannot be verified unless an actual experimental test is conducted with the proper measuring equipment. Since no such equipment is available for this thesis, it is therefore assumed these Abaqus results are accurate.

4.4.4 2.25 m x 5 m Model

As mentioned previously, the 2.25 m x 5 m model shown in Figure 4-7 is based on an existing physical prototype illustrated in Figure 1-2. Dimensions, shapes and parameters are derived from that prototype and original design. The design of this prototype mostly reflects electrical considerations, but it contains all relevant mechanical aspects.

The material used is the polyimide 2 material (see Table 2-1). Two of the three layers have copper chemically deposited on their surface. The layer with the radiating elements is without copper. It is believed that the copper would not change any of the general conclusions as its incorporation in the models changes only the material properties. The code incorporating the material properties of the polyimide material with copper in the model is more complex than that with the properties of the polyimide alone. This added complexity in the programming does not add to the scientific value of the analysis. For these reasons, the models were created using the material properties without the incorporation of the copper coating.

The 2.25 m x 5 m membrane model is analyzed using tensile loads only in this section. The results should not yield any out-of-plane deformation. The shape of the parabolic sides is calculated using the equations detailed in chapter 3 providing a uniform membrane in-plane tension throughout the layer. No wrinkle appears since the membrane has no compressive stress. As seen in section 4.1, compressive or zero stress is mandatory for the formation of wrinkles.

The boundary conditions for this model are derived from the square model in tension (section 4.4.2). Since the model is simplified by using symmetry, consequent symmetry boundaries are applied for the left and bottom sides of the model shown in Figure 4-7. The parabolic edges have the out-of-plane direction constrained on their entire length to mimic the restraint the cables are imposing on the prototype. The corner has the aluminium plate modeled as previously discussed. The nodes in this aluminium part area have the out-of-plane direction restricted since the design of that corner part prevents any movement along that axis. The thickness of the aluminium part in itself provides sufficient stiffness preventing wrinkle occurrence and justifies this last boundary constraint.

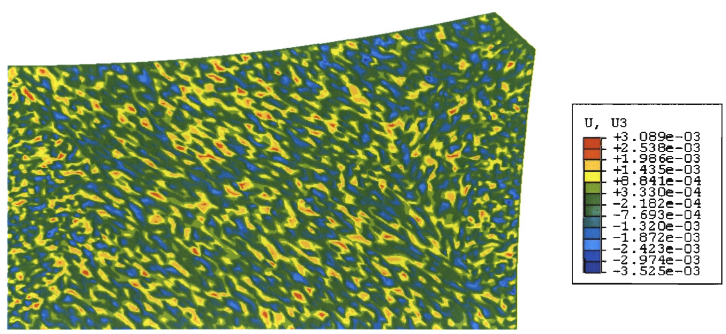

Figure 4-7 : 2.25 m x 5 m membrane out-of-plane deformation – Abaqus

Results illustrated in Figure 4-7 show out-of-plane displacements occurring all over the layer without any apparent pattern. It actually illustrates a model without any wrinkle, consistent with design calculations. The imperfections initially introduced to favour bending flatten out into a perfect plane thus creating local out-of-plane displacements proportional to these imperfections. The scale of Figure 4-7 is proportional to the value of the imperfections.

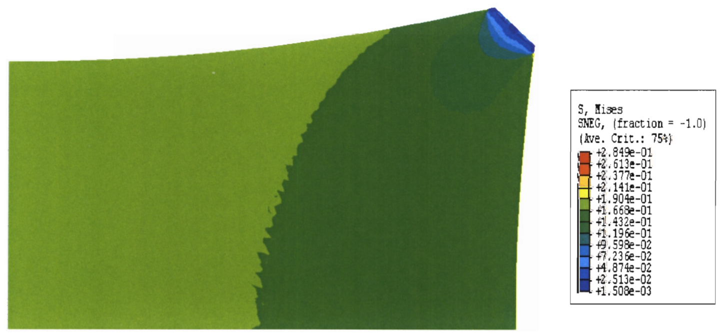

Figure 4-8 : 2.25 m x 5 m membrane stress field at design state – Abaqus

The stress field in the membrane is principally constant, as shown in Figure 4-8, respecting the design constraint. The stress throughout the membrane is around 0.172 MPa (25 psi) as designed (between 0.140 MPa and 0.190 MPa from the results scale). The impact of the corner cut-offs is immediately seen in the corners with the presence of a high stress gradient. Another design with a longer corner cut length would have a larger area affected by this stress gradient. Recalling a concern mentioned at the end of chapter 3 and illustrated in Figure 3-9 about a design with an extensive corner cut length, justifies that membrane antenna should be the focus of particular attention on wrinkling analysis. The effects of such regions with high stress gradient and their impact on the antenna design must be determined. Such concerns are not pursued further in this thesis apart from the wrinkling analysis.

This gradient is suspected of favouring wrinkle development under thermal loads considering the wrinkling criteria presented previously. That region can change to compressive stress with thermal loads. The impact of thermal loads on this design is presented in the next chapter.

5 WRINKLING ANALYSIS WITH THERMAL LOADS

Space is a harsh environment with unique peculiarities. The temperatures across a structure can vary drastically depending on whether exposed to solar radiations or not. Space environment represents one of the main challenges for spacecraft mission design.

Some observations have shown that temperature variations on a flat membrane produce wrinkles [18]. This behaviour has to be understood and accurately predicted for the expected on-orbit temperature variations of the satellite before using this type of antenna on a spacecraft. Since the membrane is preferably stretched with the minimum tension (as seen in chapter 3), the membrane material has a minimum resistance to wrinkle formation. Therefore, the thermal variations are expected to produce or at least favour wrinkles on the membrane.

The 2.25 m x 5 m membrane antenna is made of three layers linked at the corners by the support structure. Each layer has a different temperature exposure and material properties and therefore reacts differently. The expansion, or contraction, and stresses due to the thermal environment are different for each layer of the membrane. Understanding the implications of the space thermal environment on the functionality of the antenna is a driving factor for a membrane antenna design.

The finite element models developed in this thesis use the random imperfection approach. Thermal loads are added to a number of models considered in the previous chapter. The rectangular model shown in section 4.4.3 incorporates, in this chapter, thermal loads creating either heating or cooling effects over an identical area. The 2.25 m x 5 m model is subjected to the expected temperature of -40°C for a design with sunshields, to -120°C without sunshields and to special cases of the satellite projecting its shadow over a partial area of the membrane antenna while exposed to solar radiations.

From these thermal loads analyses, it will be possible and desirable to design wrinkle control features. Such design and proof of feasibility are presented in chapter 6.

5.1 Additional Assumptions for Wrinkling Analysis

Considering the addition of temperature variations in the numerical models, other assumptions had to be involved in the building of the finite element models. All assumptions mentioned in chapter 4 are also applicable for this chapter.

- The support structure of the membrane antenna is assumed to have a perfect flatness and no out-of-plane or in-plane deformation under temperature variations.
- Thermal radiation is considered to be negligible. The sun generates a constant heat flux on the membrane, therefore the temperature is not considered time dependent.
- The expansion and contraction of the cable is considered without any impact on the behaviour of the membrane layers.
- The constant-load spring is assumed to ensure the same membrane tension throughout temperature variations.
- Manufacturing and assembly of the membrane antenna are assumed to be at room temperature of 20°C.
- The parabolic shape of the cable remains unchanged when the tensioning load is applied. The design should yield the desired parabolic shape when fully stretched.

5.2 Details of the Finite Element Modeling

Presented in this section are the results of the analyses for the rectangular and the 2.25 m x 5 m models. The Abaqus code is used for all models. Both models have thermal loads included in their load case described in the previous chapter. Otherwise the models are identical. Any difference between the results presented in the present and the previous chapters are solely due to thermal loads. All displacement results are in millimetres.

The analyses shown in this section have added complexity with the thermal loads. The Abaqus code did not appear to present any difficulty in analysing the models as opposed to MSC.Nastran. The MSC.Nastran code required too many elements and iterations for the computer server's available power and memory to handle. Therefore it is not used for analysis in this chapter.

The rectangular model is analyzed for a central area being heated and again while being cooled. The final temperatures chosen for the central area are arbitrary. A non-negligible temperature variation is required for this model since only the behaviour of the wrinkle pattern is looked at. The results from temperature variations of +30°C, for the heated model and –70°C for the cooled model are presented.

A room temperature of 20°C in accordance with the manufacturing and assembly assumption is specified as the initial temperature for the rectangular model of section 4.4.3 as well as the 2.25 m x 5 m antenna model. The software calculates, with the material properties, the resulting final temperature field as well as the material expansion or contraction.

The 2.25 m x 5 m model has the initial and final temperature specified over the full membrane except for specific analyses where only a limited area has temperature variations. The thermal analyses are carried out using the Radiating Plane material properties. Wrinkle occurrence poses a greater concern on this layer by modifying the orientation of the radiating features in the electrical aperture. The out-of-plane tolerance is therefore more critical for this layer as discussed in the introduction chapter. Both the maximum and minimum temperatures shown in Table 2-8 represent a decrease from the initial room temperature.

For analyses on the 2.25 m x 5 m model, the bonded aluminium plate on the corner is included as discussed in the previous chapter. It has an impact on the local behaviour and stiffness of the model.

5.3 Finite Elements Models Results

5.3.1 Rectangular Model with Heated Area

The central area subjected to temperature variations is 120 x 156 mm and symmetrical from the center point of the model. The temperature variation of 30°C from the initial temperature of 20°C results in an applied temperature of 50°C for the central region.

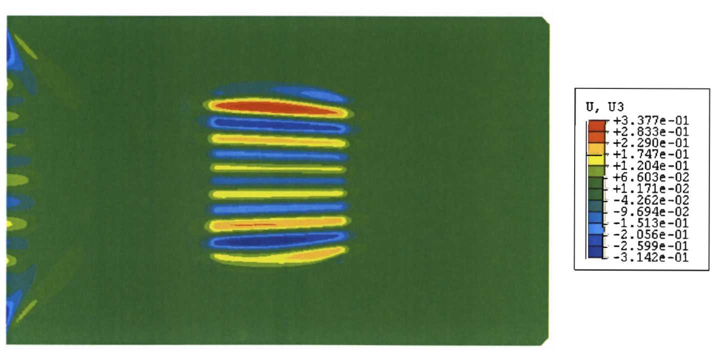

Figure 5-1 : Wrinkling of the rectangular model with a heated area

The wrinkles induced by temperature variation are evident as well as the extent of the heated area. The material of the area affected by the heat expands locally. The expanding material can only do so by wrinkling since the rest of the membrane is still being stretched by the tensile loads. These loads pull throughout the layer and orient the expanding material at the center along the horizontal axis. At the top and bottom of the central area, two main wrinkles with different out-of-plane direction are seen in Figure 5-1. The upper wrinkle comes out of the sheet while the lower penetrates into it. The out-of-plane direction, but not the height or the orientation, is dependent on the initial random imperfections initially imposed on the model. The direction has been shown to vary from one set of imperfections to another. Both directions represent valid equilibrium position. This model is without gravity loads.

The initial diagonal and left edge wrinkles are still present. Their height, numbers and orientation are unchanged. The wrinkles on the left edge have decreased in height because less tensile loads are transmitted throughout the membrane possibly by the presence of the expanding central area.

The results seem to go along with intuitively expected results, but the height and even the orientation cannot be verified unless an actual experimental test is performed and used for comparison. Until a correlation can be done between the results under thermal loads and actual wrinkles formation with a physical experiment, it has to be assumed that Figure 5-1 displays accurate results based on intuitive comparison.

5.3.2 Rectangular Model with Cooled Area

As mentioned previously, the same model is analyzed except for the final temperature of the central area. The final temperature of -50°C represents a temperature reduction of 70°C. This variation is greater than for the heated central area case.

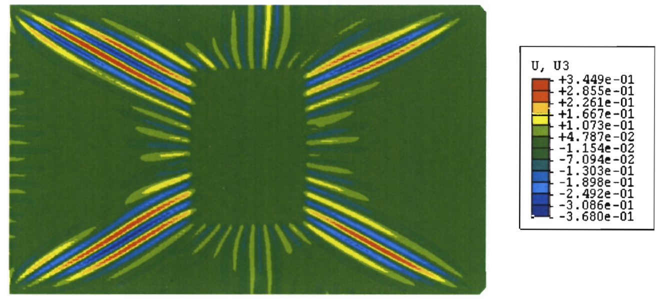

a)

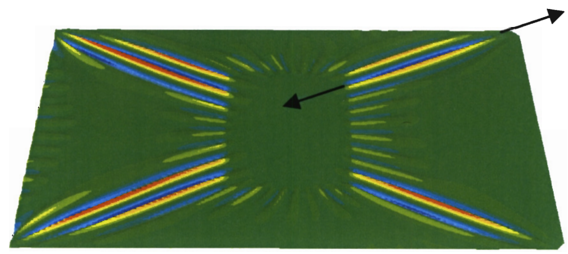

b)

Figure 5-2 : Wrinkling of the rectangular model with a cooled area

The results are evidently different but not inconsistent with the expected behaviour. The wrinkles are formed outside the central area since that region is contracting. Because that area contracts, it is stretched by greater loads than the surrounding regions. Also, since its volume decreases, the material bordering that area is being pulled together creating the wrinkles. Given that the central area pulls on all surrounding material by contracting, these wrinkles are oriented outward. This phenomenon is present and seen in Figure 5-2.

Larger wrinkles directly to and from the model corners appear explained by the presence of the initial tensile loads. In this case, the fixed left side corners have, by equilibrium, the same effect as the applied loads on the right side corners.

As the central region contracts, the resulting stress field around that area is similar to one created by hypothetical opposite tensile loads applied between the central area corners and each of the membrane corner as shown in Figure 5-2-(b). This hypothetical situation is itself similar to wrinkles produced on a flexible material being pulled at opposite sides without thermal loads as shown in a previous study [9] and illustrated in Figure 5-3.

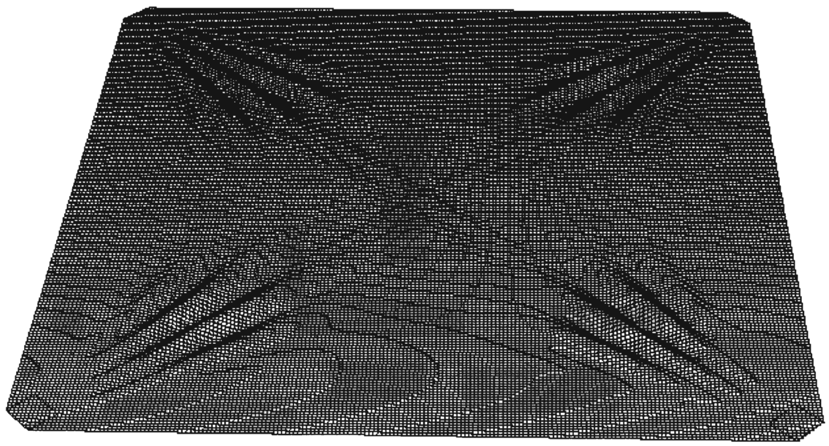

Figure 5-3 : Square piece pulled at opposite corners without thermal loads [9]

The results obtained from these three rectangular model analyses (one with mechanical loads and two with thermal loads) demonstrate the feasibility of the random imperfection approach to incorporate thermal loads using the Abaqus code. This is the main purpose of these three analyses.

None of these analyses is confirmed as yet by experimental results, essential to accept the procedure as a valid approach simulating real physical behaviour adequately.

5.3.3 2.25 m x 5 m Model

As explained previously, the emitting and receiving layer called the Radiating Plane is considered the critical layer for the 2.25 m x 5 m model design because of the presence of the radiating elements and its thermal exposure. The orientation of each emitting element toward Earth is bound by a strict tolerance. Any important wrinkle would modify the orientation of the affected emitting features and compromise their functionality.

Undoubtedly a membrane antenna would be protected by sunshields for many reasons, mechanical and otherwise. The temperatures of the antenna using sunshields are provided in section 2.4. For academic purposes, this thesis also considers the impact on the Radiating Plane with a configuration lacking such sunshields. The coldest temperature is at -120ºC for this specific analysis. Both cases, with and without sunshields, are discussed. Analyses considering the impact of the satellite shadow on the membrane antenna, a situation that occurs every orbit (depending on the type of orbit), are also presented.

5.3.3.1 Wrinkling by Temperature Variation in the Presence of Sunshields – Full Exposure

As explained previously, the membrane would be subjected to temperature variation in a space environment as described in section 2.4 from the reference initial temperature of 20ºC. The lower temperature has been rounded off to -40ºC while the highest temperature has been kept at 23ºC. The maximum temperature is not rounded off to illustrate the impact of even the smallest temperature variation.

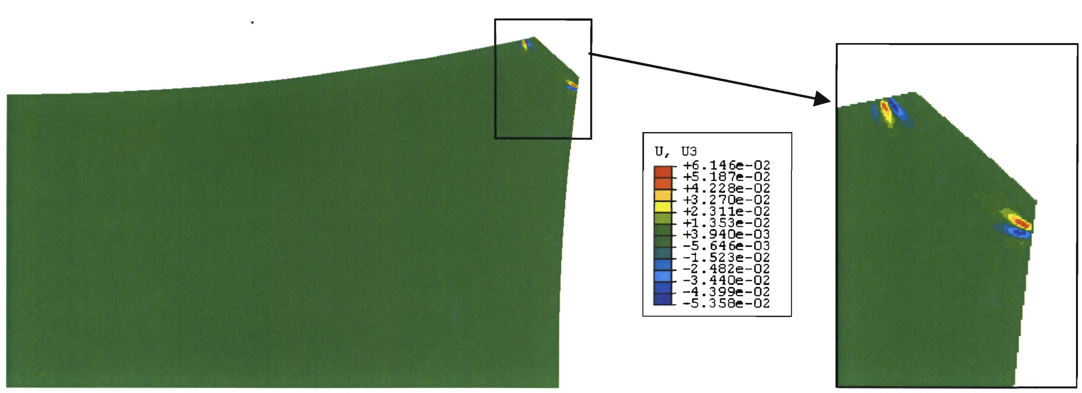

a) 23°C

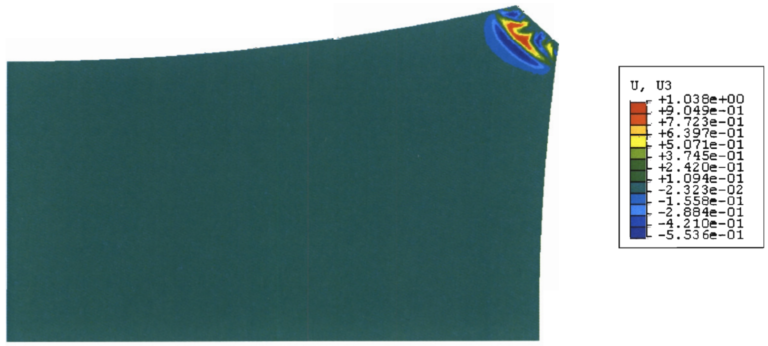

b) -40°C

Figure 5-4 : Wrinkling of the 2.25 m x 5 m model with sunshields by temperature variation

The positive temperature variation to 23°C, representing an increase of 3°C, is enough to initiate wrinkle formation as shown in Figure 5-4-(a). Wrinkles form near the aluminium plate at the end of the parabolic edges. Figure 4-8 shows the stress field of the 2.25 m x 5 m model without thermal loads as well as a gradient near the corner cut-off. The thermal loads modify the stress field enough for zero (or compressive) stress to occur creating these wrinkles.

These wrinkles have no impact on the functionality of the antenna because they are outside the central electrical aperture. It is expected that for a slightly different membrane shape and cable load design, these wrinkles would be similarly acceptable. Therefore the impact of this temperature increase is negligible.

Figure 5-4-(b) shows the result of the decrease in temperature on the planarity of the membrane. The deformation, or wrinkled area, is localized in the corners.

Since the functionality of the antenna is dependent on the planarity of the rectangular electrical aperture, the wrinkling of the corner areas is not critical and can be acceptable. On the other hand, if a specific shape design has the corner cut-off closer to the electrical aperture (as would be for an optimum configuration to reduce the size of the support structure as explained in chapter 3), then the local wrinkles could overstep into the aperture area and affect some radiating elements. This conclusion accentuates the importance of wrinkling analysis for all designs, even with sunshields.

5.3.3.2 Wrinkling by Temperature Variation without Sunshields – Full Exposure

The removal of the sunshields would yield temperatures of +120°C and –120°C for the studied membrane layer. Interestingly, the difference between results with and without sunshields is relatively minor when considering the area affected by wrinkles as shown in comparing Figure 5-4 and 5-5Figure 5-5. The height is of course proportional to the magnitude of the temperature variation, and it can be shown that it increases consistently with the decrease in temperature.

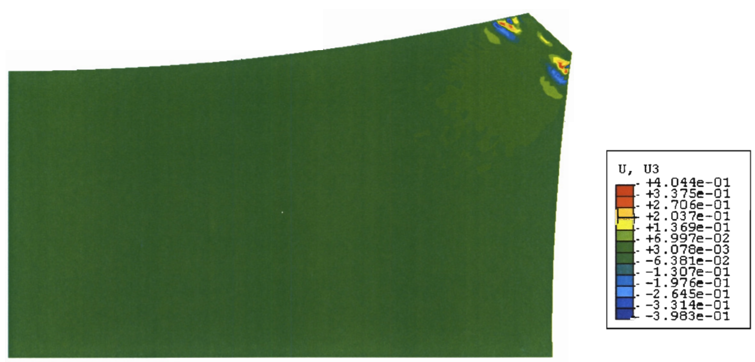

a) +120°C

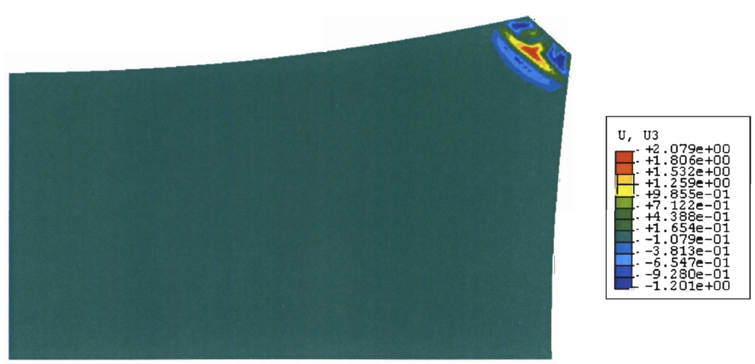

b) -120°C

Figure 5-5 : Wrinkling of the 2.25 m x 5 m model without sunshields by temperature variations

From a purely mechanical point of view, the sunshields could be removed for this design since the wrinkle-affected area does not encroach on the electrical aperture. For electrical considerations, the sunshield is a critical component of the antenna.

5.3.3.3 Wrinkling by Temperature Variation in the Presence of Sunshields – Partial Exposure

An orbiting satellite has different phases of sun exposure. The satellite, while always facing Earth, constantly changes its orientation with respect to the sun while orbiting the Earth. The satellite bus, or main structure, depending on the chosen orbit, could project a shadow onto its own antenna. This shadow alters the temperature field, which becomes non-uniform.

As seen previously, a non-uniform temperature field, i.e. presence of a temperature gradient, favours wrinkle appearance by modifying the stress field and possibly allowing zero stresses to appear.

The symmetry used for the 2.25 m x 5 m model cannot be justified with a shadow condition since it can occur anywhere and not necessarily in a symmetrical position. A full 2.25 m x 5 m finite element model is used for this analysis.

The temperatures chosen for the analyses are the same as those used in the previous sections with the presence of sunshields. The entire antenna is simulated as being fully exposed of the sun at 23°C while the shadow of the satellite bus on the antenna imposes on that region a temperature of -40°C. These temperatures represent hypothetical values for this analysis since no complete thermal study has been done for this specific case as was for other cases [17].

The dimensions of the shadowed area projected on the membrane antenna are unknown since the satellite dimensions are themselves undetermined at this time. The use of a 1 m x 1 m satellite bus is being proposed [17]. These dimensions are directly used as the shadow of the satellite. Irrespectively of the correct dimensions of the bus, general conclusions drawn from the results of the analysis are valid for any size of the shadow.

The wrinkling pattern obtained is similar to the rectangular model with cooling on its central area as described in section 5.3.2. The material in the satellite shadow contracts and pulls on the surrounding material in the same fashion as described in section 5.3.2 and creates the wrinkles oriented outward.

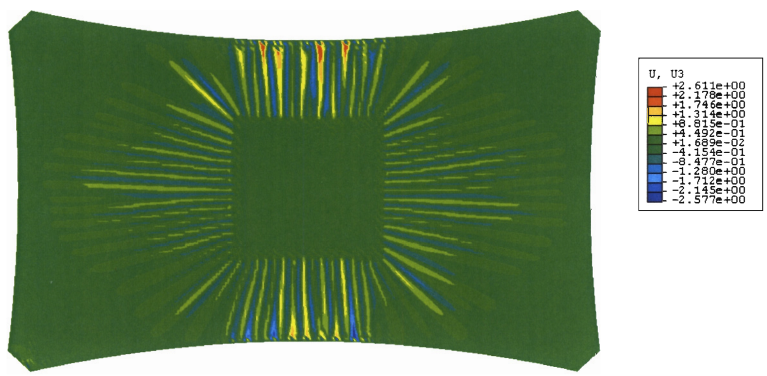

Figure 5-6 : Wrinkling of the 2.25 m x 5 m model with sunshields under full sun exposure and a 1m x 1m satellite shadow at the centre

The wrinkles produced by the satellite shadow can occur anywhere on the membrane layer. This causes concerns from an electrical point of view since when these conditions prevail, the affected areas become unstable and useless if the wrinkle heights are outside deformation tolerances. The functionality of the radiating elements in the wrinkle-affected region is compromised, undermining the performance of the radar.

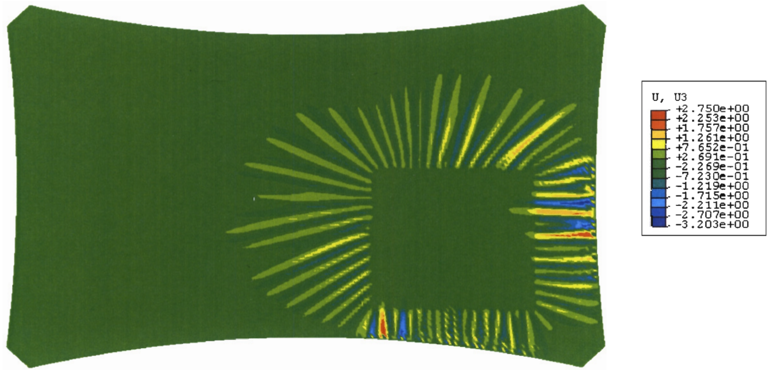

Figure 5-7 : Wrinkling of the 2.25 m x 5 m model with sunshields under full sun exposure and a 1m x 1m satellite shadow in an asymmetrical position

These analyses clearly show compatibility with previously obtained results for the rectangular model. They form the basis from which it is believed that a membrane antenna subjected to simultaneous partial heating and cooling, from exposure to the sun and the satellite shadow, produces similar wrinkles inside its electrical aperture.

For a membrane affected by wrinkles surpassing the out-of-plane deformation tolerance, the solution of increasing the in-plane tension of the design must be considered. The increased in-plane tension would reduce the area affected by zero or compressive stress by increasing the positive stress throughout the membrane. It would also help reduce the wrinkles height.

While some wrinkles occurring on the SAR membrane antenna are acceptable, others are not and create concerns. Theses analyses must be done to determine the acceptability of these wrinkles for any membrane shape design.

The results on the wrinkle pattern and orientation obtained and presented within this chapter are consistent with expectations. However, establishing the accuracy of the results regarding the wrinkle height requires a correlation with experimental tests. The resources required to conduct such tests and measurements were not available for this thesis.

6 FEASIBILITY OF WRINKLE CONTROL FEATURES

The wrinkling of the 2.25 m x 5 m membrane antenna model under tensile and thermal loads has been shown in the previous chapters to concentrate in the corners for a uniform temperature field. The formation of wrinkles in the corners is not problematic, as it does not encumber the functionality of the radar antenna. These wrinkles form under full exposure to the lowest temperature of -40°C. The stress field obtained prior to applying a temperature variation has the greatest gradient in the corners as seen in Figure 4-8 which explains the presence of compressive or zero stress as a result of thermal variation in the membrane.

Chapter 3 discusses the mass and cost advantages and disadvantages of a design for the corner cuts to be as close to the electrical aperture as possible. Another shape design than the studied 2.25 m x 5 m model with the corner cut-offs moved inward, i.e. toward the electrical aperture, would allow a smaller and lighter membrane as well as a smaller and lighter support structure. However, the wrinkles shown in section 5.3.3.1 could overlap the electrical aperture. The modified orientation of the radiating elements of the wrinkle-affected area would possibly compromise the electrical performance of the antenna. They could become useless when these thermal circumstances exist.

A method for reducing the size of the wrinkle-affected area involves increasing the membrane in-plane tension as discussed in chapter 5. Since this solution implies increasing the cable load and consequently increasing the required stiffness and weight of the support structure, the alternative option is accepting the presence of wrinkles by either controlling their orientation outside the electrical aperture or by reducing their height within tolerance. The control of the height and orientation of the wrinkles is accomplished by features added to the tensioning mechanism in the corners of the membrane antenna.

Passive designs for such controlling features are developed to reduce the extent of the wrinkle-affected area and reorient the wrinkles by modifying the stress field. These allow the corner cuts described in chapter 3 to be closer to the electrical aperture and therefore reduce the size of the membrane antenna and the weight of the support structure.

This chapter presents the results of the study on the feasibility of controlling the orientation and height of the wrinkles as well as the size of the area affected. Different designs are examined and discussed supporting this feasibility. They modify the stress field by adding loads, holes or slots. Three examples are shown demonstrating the effectiveness of a passive approach to controlling wrinkles. Since only the feasibility is of interest here, no optimisation scheme for such wrinkle control is conducted.

6.1 Assumptions for the Control Feature Designs

As explained in the next section, previously used numerical models are modified for the analyses of this chapter. These modifications require additional assumptions. All assumptions mentioned in chapter 5 are also applicable for this chapter.

- The weight and stiffness of the added parts of the designs presented in this chapter are neglected.

- The contraction of the wire or strip is correctly simulated by equivalent loads. The membrane in-plane tension prevents the layer material displacement under the wire or strip contraction. The stress equations used are for bars or plates with fixed ends.

6.2 Details of the Finite Element Modeling

The numerical model presented in section 5.3.3.1 is used to implement the passive wrinkle control designs. Therefore all loads and boundary conditions for the membrane are identical as in section 5.3.3.1.

The manufacturing and assembly of the antenna are assumed to have been completed at a room temperature of 20 °C as mentioned previously. The maximum temperature the membrane is subjected to in a space environment is 23°C. The lowest temperature, rounded off to -40°C represents a change of 60°C.

The results of the analyses for all control feature designs are compared in height, pattern and orientation of the wrinkles with those without control presented in Figure 5-4 and shown again in Figure 6-1.

The wire, or strip, is simulated by a 0.05 N load. This added load on the holes or slot is implemented as equivalent concentrated load on the inner surface of the attachment point of the wire or strip as detailed in the next section.

6.3 Wrinkles without Control Features

The results of Figure 6-1 have already been shown in section 5.3.3.1 and will be used as the baseline to compare the impact of the wrinkle control features.

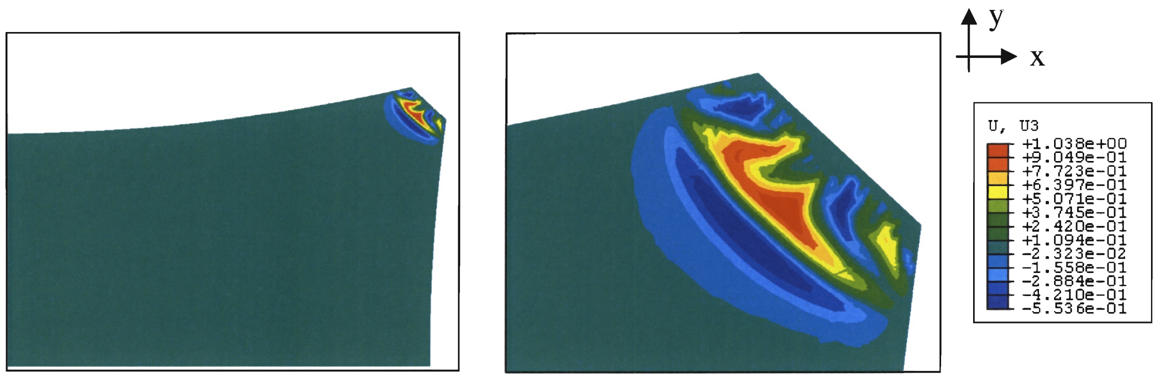

Figure 6-1 : Wrinkling of the 2.25 m x 5 m model at -40°C

The stress field obtained for this temperature and load state has not been presented previously. Since the following discussions underline the modification of the stress field by the wrinkles control features, the von Mises stresses are shown below as well as the major and minor principal stresses in accordance with discussions on wrinkling criteria in section 4.1.

The coordinates system shown in the previous figure is relevant to all figures in this chapter.

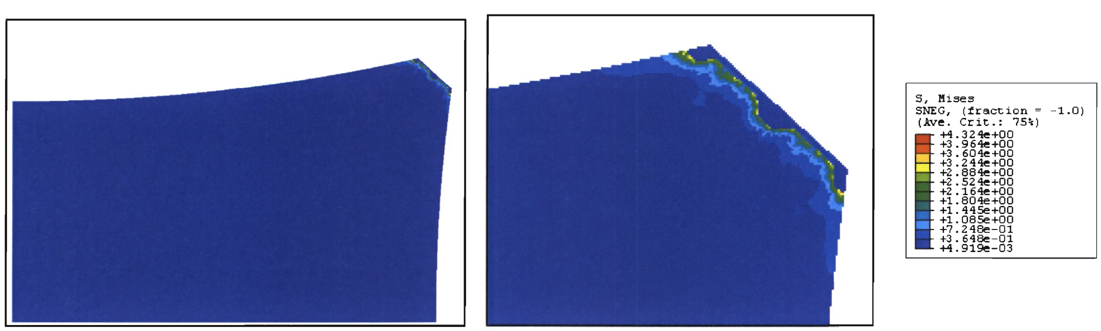

Figure 6-2 : Von Mises stresses in the 2.25 m x 5 m model subjected to a -40°C temperature

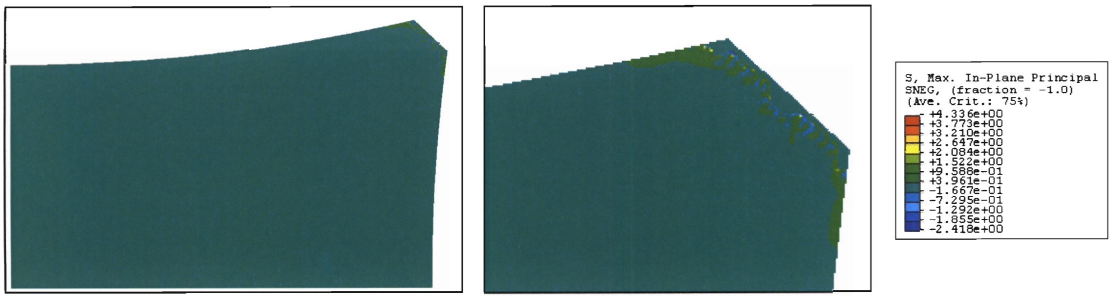

Figure 6-3 : Major principal stresses of the 2.25 m x 5 m model subjected to a -40°C temperature

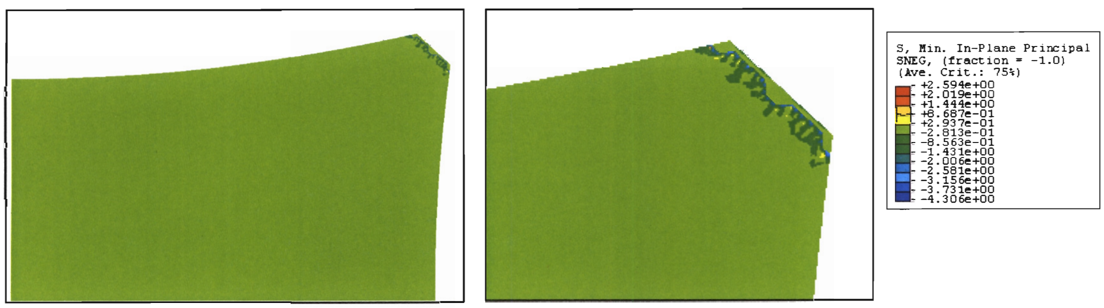

Figure 6-4 : Minor principal stresses of the 2.25 m x 5 m model subjected to a -40°C temperature

In accordance with discussions in section 4.1 on wrinkling criteria, Figure 6-3 showing the major principal stresses accounts for tensile stresses in the whole membrane while Figure 6-4 demonstrates the presence of compressive stresses in the minor principal direction in the membrane. The influence on the stress fields of the aluminium corner part can be seen in these figures.

6.4 Design 1 – Tensile Loads on Hole Cuts

This design features two different characteristics; holes cut in the membrane and a tensile load applied on these holes. The design simulates two wires, or strips of material, connected on the aluminium plate, called the stiffener, and tied on the other end to a 0.125 in (3.175 mm) diameter hole. Two holes are cut in the membrane, therefore two wires are integrated. Each wire, or strip, contracts under the temperature drop creating a load on the attached hole in the direction of the wire. They are simulated in the model by loads of 0.05 N applied at a 45° angle as shown in Figure 6-5. Each load is replaced by an equivalent distributed load on the nodes of the proper half of the hole cut. The positions of the cuts are arbitrary. The combination of the position of the holes and the magnitude of the load is found by a trial and error method. As explained earlier, the purpose for these analyses is not the optimisation of the designs but the proof of the feasibility of controlling wrinkles.

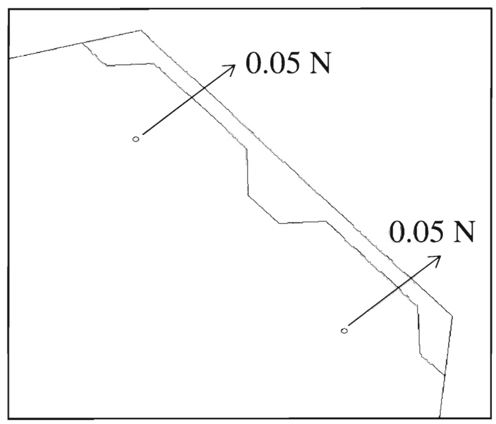

Figure 6-5 : Control feature design 1 – tensile loads on hole cuts

The impact of this passive wrinkle control design shown in Figure 6-6 is distinctly evident compared with the initial state recalled in Figure 6-1. This passive approach for controlling the wrinkles modifies their pattern, orientation and height. In addition, near the electrical aperture, the wrinkle heights have decreased. The new pattern of the wrinkles has completely changed their orientation and number. However, the extent of the area affected is similar.

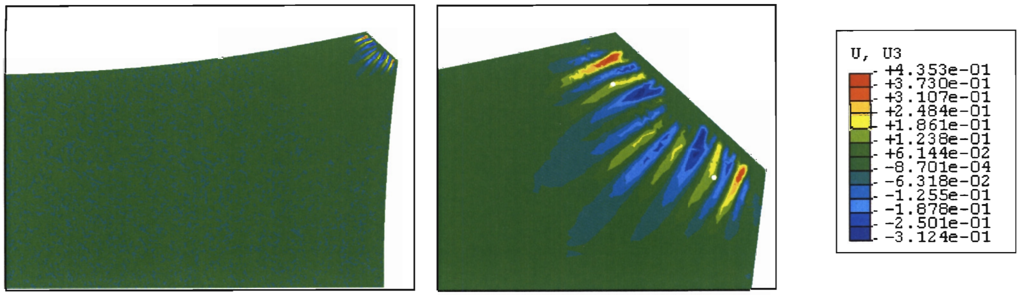

Figure 6-6 : Wrinkling of the 2.25 m x 5 m model with control feature, design 1

This design decreases the wrinkle height in one out-of-plane direction by 58 % from 1.038 mm to 0.4353 mm and by 43.6 % from 0.5536 to 0.3124 mm in the other out-of-plane direction. The impact of this design on the wrinkles is not negligible and presents noticeable advantages.

For other membrane shape designs than the 2.25 m x 5 m membrane antenna model, there is a likeliness these corner wrinkles would overstep in the electrical aperture area. This design could reduce the wrinkle heights to an acceptable level avoiding a complete redesign of the membrane shape, in-plane tension and cable load.

This passive design acts by altering the stress field as discussed previously. The following figures display the von Mises stress field, the major principal stresses and the minor principal stresses. The wrinkles are initiated by the presence of compressive, or negative, stresses in the minor principal stress field.

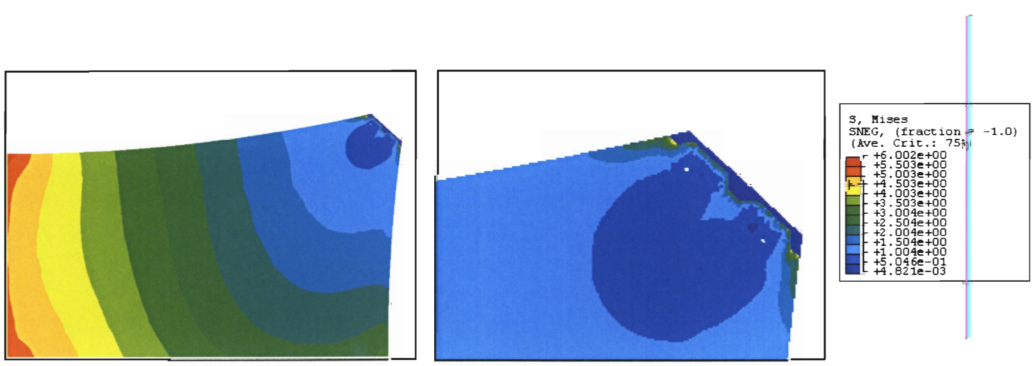

Figure 6-7 : Von Mises stresses of the 2.25 m x 5 m model with the control feature subjected to a -40°C temperature - design 1

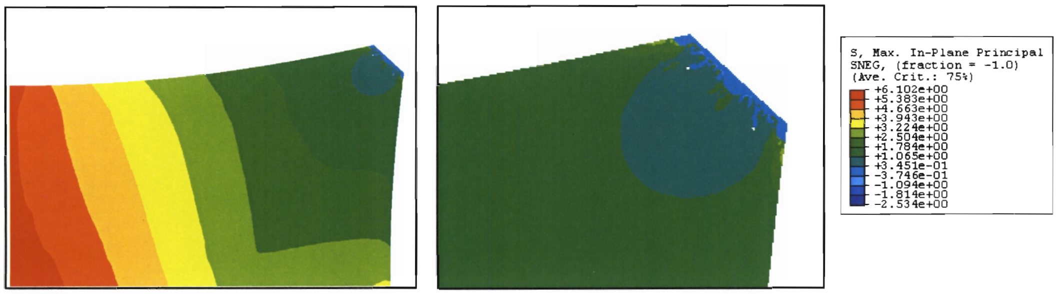

Figure 6-8 : Major principal stresses of the 2.25 m x 5 m model with the control feature subjected to a -40°C temperature - design 1

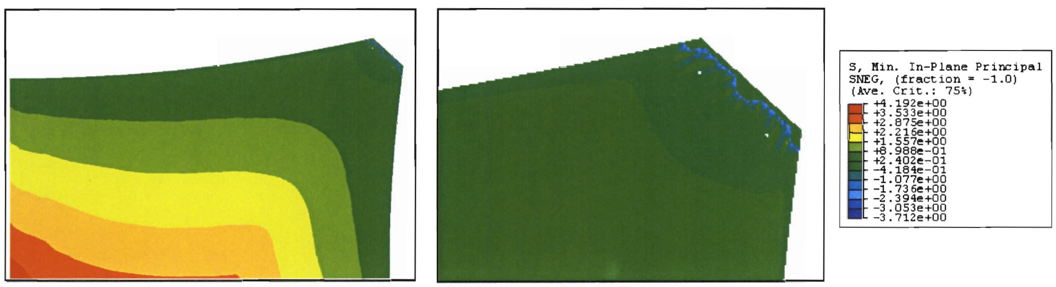

Figure 6-9 : Minor principal stresses of the 2.25 m x 5 m model with the control feature subjected to a -40°C temperature - design 1

6.5 Design 2 – Tensile Loads on Straight Slot Cuts

This second design introduced to control wrinkling in the corners of the membrane antenna is identical to the previous one except that it uses slots instead of holes. The slots are 0.5 in (12.7 mm) wide. The orientation and length of the slots are arbitrary and a trial and error method reveals a satisfactorily set of these characteristics. Wires or strips of material attached on the aluminium plate and connected at the slots end are simulated by a 0.05 N load at a 45° angle applied as shown in Figure 6-10. The loads are replaced by equivalent concentrated loads on the appropriate nodes of the slots rounded end.

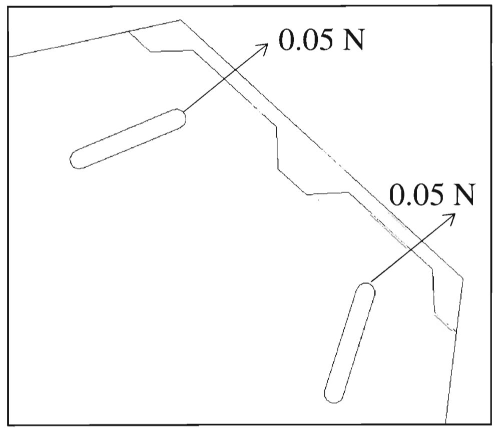

Figure 6-10 : Control feature design 2 – tensile loads on slot cuts

The wrinkle pattern obtained for this control feature shows a different configuration from the initial state and also from the use of the design presented in Figure 6-6. Figure 6-11 shows that the size of the wrinkle-affected area decreases with the use of this design. The advantage offered by this specific design acts on the control of the orientation of the wrinkles along the slots.

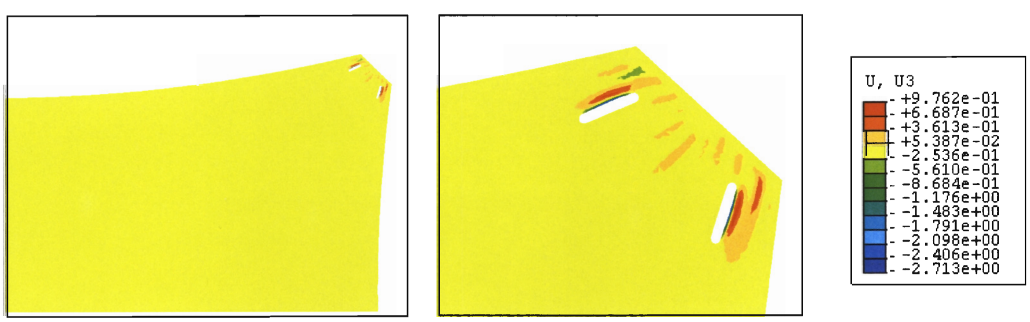

Figure 6-11 : Wrinkling of the 2.25 m x 5 m model with control feature, design 2

Since the wrinkles occur mostly next to the slots, this design allows the orientation of the wrinkles in a desired direction toward low impact areas. This design could allow reducing the size of the antenna by moving the corner cut edges inward toward the electrical aperture while orienting the wrinkles outside that critical area.

6.6 Design 3 – Tensile Load on a Hole Cut with a Parallel Slot

The slot in this design is parallel to the corner cut edge at an arbitrary distance. The slot is 3.175 mm wide (1/8 in). The hole connecting the wire or strip is 3.175 mm (1/8 in) in diameter. A load of 0.05 N applied at a 45° angle on the nodes of the appropriate half of the hole cut simulating the same wire or strip design as the two previous designs. No force is applied on the slot. Its only use is limiting the extent of the wrinkle-affected area.

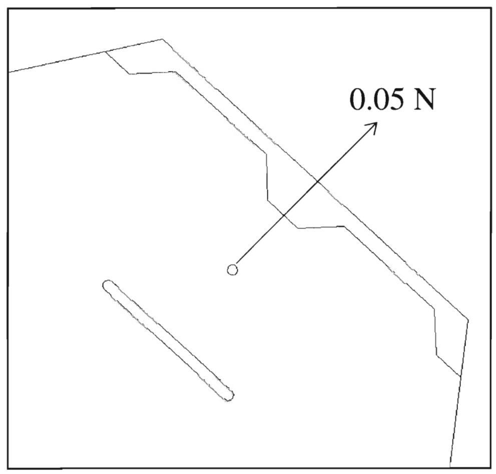

Figure 6-12 : Control feature design 3 – tensile loads on a hole cut with a parallel slot

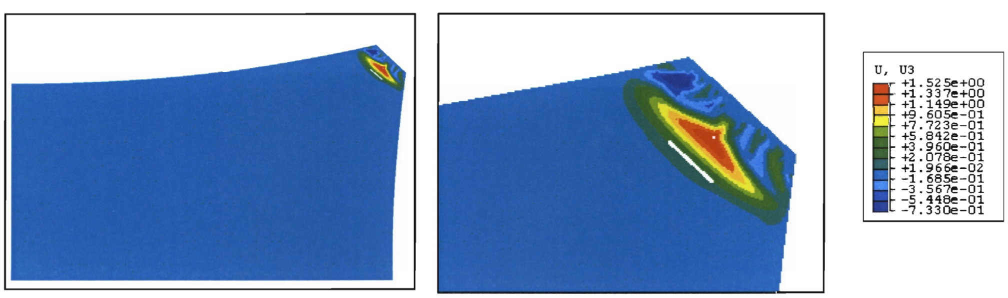

Figure 6-13 : Wrinkling of the 2.25 m x 5 m model with control feature, design 3

The tensile load applied on the hole helps restricting the wrinkle-affected area between the slot and the corner edge.

The wrinkle height in the one out-of-plane direction increases by 46.9 % to 1.525 mm. The height in the other out-of-plane direction also increases by 29.4 % to 0.733 mm.

The size of the wrinkled area decreases and seems to be contained by the parallel slot introduced. Since the wrinkles are controlled and forming outside the aperture, this design is to be considered. However, concerns over the efficiency of such slot for containing the affected area are raised for other membrane shape designs and slot position. For example, the effect of bringing the slot closer to the corner edge on containing the affected area is unknown.

6.7 Wire and Strip Calculations

It has been initially assumed that wires or strips of material could be used in the designs presented previously in this chapter as loads of 0.05 N. Materials with the proper coefficient of thermal expansion would allow engineers to use this suggested approach in controlling wrinkles.

The calculations for finding the corresponding wire diameter of different materials yielding 0.05 N at -40°C were done [24]. These calculations found that metals and polymers are not possible materials since their resulting diameters are too small and could not physically be implemented on the antenna.

The calculation for finding the corresponding strip width for different materials for the same load and temperature parameters were also done. These calculations found that it was possible to use the polyimide 2 material (see Table 2-1) for the wrinkle control features. Since this material is already used in the making up of the membrane antenna itself, it would be available.

All detailed calculations and results are presented in Appendix C.

7 DYNAMICS ANALYSIS

The analyses presented in the previous chapters on the membrane antenna considered the 2.25 m x 5 m model. It is a prototype, a model built toward the full development of this technology. A flight design for a space mission requires a larger antenna size for electrical requirements.

A membrane design of 2.25 m x 10 m is considered for possible future flight opportunities [17]. Considering the on-orbit micro-vibrations and the out-of-plane deformation tolerances (see chapter 2), conducting dynamic analyses with the flight antenna dimension becomes crucial, especially with a large and flexible membrane. The membrane antenna is expected to have a non-negligible response to the on-orbit micro-vibrations occurring during all operational cycles of the satellite. Another motivation for use of the 2.25 m x 10 m model lies in data from previous analyses, made by an external source and available for comparison [17]. For these reasons, the natural frequency analyses and frequency response analyses focus on the proposed 2.25 m x 10 m model dimensions. This membrane antenna shape designs is used for all dynamic analyses.

It has been determined that the first natural frequency of the membrane must be higher than 2 Hz as discussed in chapter 2. Any lower frequency could result in problems during operation in orbit. Since each layer is independent and has different material properties as discussed in section 2.1 on different copper covered surfaces, each has its own natural frequency and has to be looked at separately.

The electrical functions of the antenna can use different radio signal wavelengths to operate. This thesis studies the impact of two potential flight design wavelengths for the antenna radar; the L-Band and C-Band configurations. The difference, from the mechanical point of view, resides in the number and spacing of the radiating elements on the Radiating Plane. A C-Band configuration uses approximately 4 times the number of elements of the L-Band configuration. An L-Band configuration requires the element spacing to be at 93.75 mm and the C-Band at 22.1 mm. Behind each radiating element comes a strip of material attached to the Radiating Plane and Feed Network Planes. These strips of material used for electrical functions are replaced in the finite element models by small masses at predetermined locations on these two layers.

Determining the natural frequency becomes important when considering the membrane antenna within the complete satellite structure. The satellite itself and its sub-systems inevitably produce micro-vibrations within a precise frequency range. Since the membrane antenna has an out-of-plane deformation tolerance, the dynamic amplification of the antenna must be studied. Out-of-tolerance deformations could result from dynamic amplification of the satellite vibrations with a natural frequency of the antenna close to the excitation frequencies.

The frequency response analyses study this amplification to on-orbit micro-vibrations. External sources have determined the excitation levels as shown in Table 2-10. The maximum displacements from the frequency response analyses are presented for both wavelength configurations. No temperature variation is considered in this chapter.

7.1 Assumptions for Dynamic Analysis

- It is assumed that the adhesive tape between each polyimide material sheet on each layer does not influence the dynamic behaviour in any circumstance.

- It is assumed the constant-load spring in the tensioning mechanism does not affect the dynamic behaviour of the antenna.

- The parabolic shape of the cable remains unchanged when the tensioning load is applied. The design should yield the desired parabolic shape when fully stretched.

- The sliding of the cable is considered to be perfect, without friction, preventing any shear load to be transmitted to and from the membrane.

- The support structure of the membrane antenna is assumed to have a perfect flatness and no out-of-plane or in-plane deformation.

7.2 Details of the Finite Element Modeling

This finite element model is analyzed solely in MSC.Nastran. This software is used because previous analyses are available for comparison [17]. The numerical model is composed of three layers. Each layer is independent since it is directly attached to four fixed rigid beams simulating the support structure. The cables stretching each layer are modeled as opposite to the models analysing the membrane wrinkles. The sliding characteristic of the cable with the membrane edges is modeled with the Multi-Point Constraint (MPC) option of the software. This characteristic prevents any shear load from transmitting from the cable to the membrane and vice-versa. Each layer has its own material properties including the copper chemically deposited. The Radiating Plane material properties are representative of the polyimide 3 material (see Table 2-1). The Ground Plane has 100 % of its surface coated with copper. The Feed Network Plane has 75 % of its surface covered by copper with the L-Band configuration and 90 % with the C-Band configuration as discussed in section 2.1. This difference comes from electrical requirements outside the scope of this thesis.

The corner cut-offs are modeled. The finite element model does not include the tensioning system design as shown in Figure 1-2, apart from the cables. The complexity of the mechanism and parts of the tensioning system do not add to the relevance of the results. This tensioning system has instead been replaced by equivalent loads and boundary conditions. Replacing the tensioning system is realized by four added attributes. First, because the tensioning system is not included in the model, the cables, which should have stopped at this tensioning system, are extended to the support structure with modified properties (explained further). Second, a boundary condition restricting the out-of-plane displacement of the corner cut edge replaces in the model the natural restriction the tensioning system has on the membrane. This constraint is imposed on the (x_1, y_1) and (x_2, y_2) points (see section 3.2.3). Third, the equivalent loads of the tensioning system are applied axially on the cable at the end of the parabolic edges. For equilibrium purposes, the resultant load for each corner is applied at the cable intersection (see Figure 7-1) on the support structure. Fourth, the segments of the cable extended from the parabolic edge ends to the support structure have reduced properties (reduced section area and Young's modulus). Otherwise, the stiffness of these segments would alter the dynamics results. It is expected (and has been shown) that some in-plane modes result from this modeling approach. These modes are in-plane since the corners of the membrane have the out-of-plane direction constrained. These in-plane modes are removed leaving the correct membrane modes to be analyzed. These added attributes allow simplifying the model and opt out the details and complexity of the tensioning system.

The support structure, which is yet unknown, is bound to have an impact on the dynamic behaviour of the membrane but cannot be taken into consideration for the analysis of this thesis. No type of such structure, such as telescopic booms or inflatable structures has been included in this study. Each type could have a different impact. It has been decided to neglect its effect altogether.

The partial support structure modeled has over-stiffed properties preventing any sizeable impact on the dynamics results. The support structure has all degrees of freedom restricted at its free ends seen in Figure 7-1.

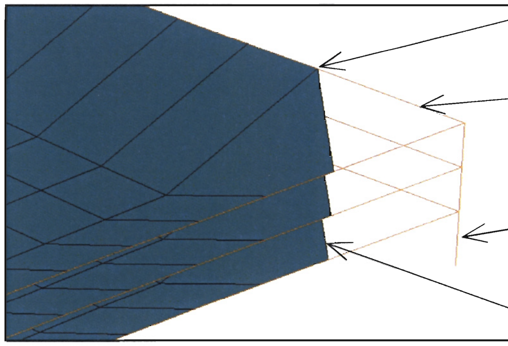

Figure 7-1 : 2.25 m x 10 m cable modeling

Mass-points are added to the model to simulate the components linking the Radiating Plane to the Feed Network Plane for each radiating element. As mentioned, the C-Band configuration has approximately 4 times the number of emitting elements (or simulated masses) than the L-Band configuration. The tensioning system has been replaced with an equivalent mass-point at each of the corners.

The models use CQUAD4 elements for the membrane layers, CBAR elements for the cables and an over-stiffed beam property for the support structure. The added masses are modeled with CONM2 mass-point properties. The copper properties on the appropriate layers are simulated using the PCOMP option of the MSC.Nastran software. The connections between the cables and the layers have been modeled using multi-point constraints, or RBE2 constraints.

7.3 Natural Frequency Analysis

Each layer has the same cable load and membrane tension, but different material properties yield different natural frequencies. The natural frequency is a function of the stiffness and mass of the layer, which explains this expected difference.

7.3.1 L-Band Membrane Configuration

Each layer has the same mode shape occurring at different frequencies. The shapes of the modes have been determined with an eigenvalue analysis. The first and second mode shapes are shown in Figure 7-2-(a) and (b), respectively.

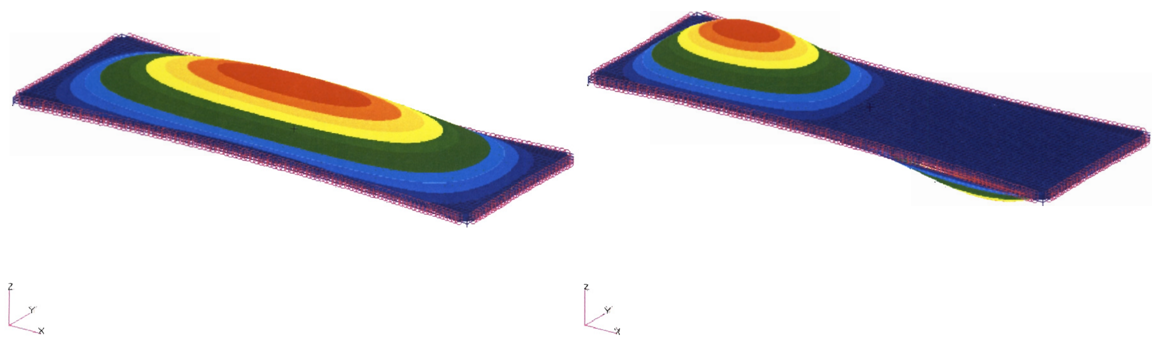

a) First mode shape **b) Second mode shape**

Figure 7-2 : 2.25 m x 10 m typical mode shape for the L-Band configuration

The first natural frequencies of the Ground and Feed Network Planes, both covered with copper are lower than the Radiating Plane as seen in Table 7-1. The lowest first natural frequency is 1.574 Hz for the Feed Network layer. The difference between the first natural frequencies of the Ground and Feed Network Planes can be explained by the difference in copper mass (see Table 2-2) and layer stiffness. The Ground Plane has its entire surface coated with copper, differing from the Feed Network Plane. The resulting stiffness and mass of the planes are, in consequence, different as discussed previously.

Membrane Layer	First Natural Frequency [Hz]	Second Natural Frequency [Hz]
Radiating Plane	5.510	8.013
Ground Plane	1.582	1.906
Feed Network Plane	1.574	1.896

Table 7-1 : Membrane antenna natural frequencies for the L-Band configuration

The first natural frequencies of the Ground and Feed Network Planes are lower than the given 2 Hz limit. This represents a problem. These layers would dynamically amplify micro-vibrations from a specific component, the Attitude Control System [17].

Since the parameters influencing the natural frequencies of the model are the mass and the stiffness and since modifying the mass is not desirable, one solution is to increase the 50 psi (344.7 kPa) in-plane tension for this configuration. It would increase the first natural frequency of all layers above the 2 Hz limit.

7.3.2 C-Band Membrane Configuration

The natural frequencies for the C-Band membrane are expected to be higher than for the L-Band since the copper thickness is half the corresponding thickness on the L-Band configuration. This difference is dictated by electrical needs. However, for the Feed Network Plane, the extent of the area coated with copper is raised to 90 % for the C-Band configuration compared with 75 % for the L-Band configuration.

The first and second mode shapes for all layers are similar and illustrated in Figure 7-3.

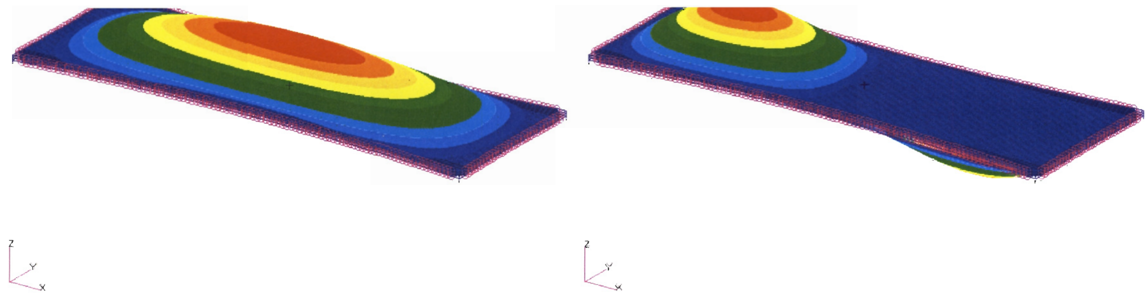

a) First mode shape **b) Second mode shape**

Figure 7-3 : 2.25 m x 10 m typical mode shape for the C-Band configuration

The first natural frequency of the Radiating Plane has decreased to 4.107 Hz from the 5.510 Hz for the L-Band configuration. Mass is the factor responsible for this difference resulting from the growth in the number of mass-points simulating the radiating elements.

The increase of the natural frequencies of the other planes is generated mainly by the decrease in mass (compared to the L-Band case) rather than the stiffness change.

Membrane Layer	First Natural Frequency [Hz]	Second Natural Frequency [Hz]
Radiating Plane	4.107	5.219
Ground Plane	2.133	2.585
Feed Network Plane	2.053	2.485

Table 7-2 : Membrane antenna natural frequencies for the C-Band configuration

The Ground and Feed Network Planes for the C-Band configuration have their first natural frequency of 2.133 Hz and 2.053 Hz, respectively. These values are above the 2 Hz lower limit satisfying the design constraint.

7.4 Frequency Response Analysis

While in orbit, a satellite is subjected to different micro-vibrations from many sources. A membrane antenna is especially susceptible to dynamic amplification of these micro-vibrations. As seen in the previous section, the first natural frequencies of the layers are in the same frequency range as these vibrations detailed previously (see Table 2-10).

Results of the frequency response analyses of the displacement caused by on-orbit micro-vibrations for both L-Band and C-Band configurations are presented. Their differences are examined in this section.

An important parameter in any frequency response analysis is the modal damping ζ or the quality factor Q ($Q \approx 1/2\zeta$). For composite structures, a value of 30 for Q is standard in analysis [17]. For a purely metallic model, a higher Q is used in dynamic analyses. The polyimide material used in the design has a damping factor that is not known. This lack of knowledge raises concerns and poses a challenge for the desired analyses.

The damping can be determined by tests on a physical prototype but the results would be greatly corrupted by air damping acting on the membrane layers. An educated and experienced guess puts the value of Q at 10 [17][19]. It is not known if the actual Q is lower or higher. Resources were not available to perform the required physical tests and measurements to establish the correct value for the quality factor Q.

The dynamics analyses presented in this thesis are repeated for three different quality factor (Q) values; 5, 15 and 30. The quality factor Q is not expected to be lower than 5 because of the high damping this value represents ($\zeta \sim 1/2Q$). The known Q value of 30 for composite structures is chosen to limit the possible range at the higher end. An intermediate value of 15 for Q is also included in the analyses.

The frequency response analyses are carried out for frequencies lower than 3 Hz in accordance with the information available and shown in Table 2-10. The excitation level over the 3 Hz limit decreases rapidly to the zero level excitation and is therefore neglected. For analysis purposes, the 0.01 g level is kept constant for all frequencies.

7.4.1 L-Band Membrane Configuration

The out-of plane tolerance for the L-Band wavelength configuration allows a displacement of 10 mm as seen in Table 2-9.

Figure 7-4 outlines the importance of determining and using the correct value of the quality factor Q. For a Q value of 5, the maximum displacement of 7.94 mm satisfies the 10 mm tolerance. A higher value of Q = 15 results in an out-of-plane maximum displacement for the Feed Network and Ground Planes of 24.07 mm and 23.82 mm respectively. These displacements are twice the acceptable tolerance, rendering the antenna unusable at all times and therefore unacceptable.

Since the Ground and Feed Network Planes have similar mass and stiffness, they have comparable behaviour while subjected to the 0.01 g vibration level resulting in two coinciding results lines in Figure 7-4-(a), (b) and (c).

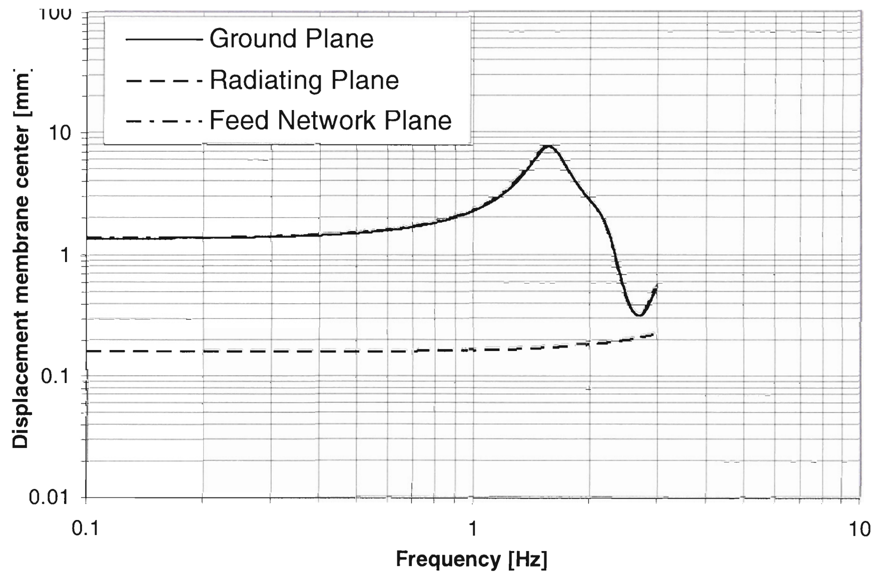
Ground Plane
Radiating Plane
Feed Network Plane
Displacement membrane center [mm]
100
10
1
0.1
0.01
0.1
1
10
Frequency [Hz]

a) Q = 5

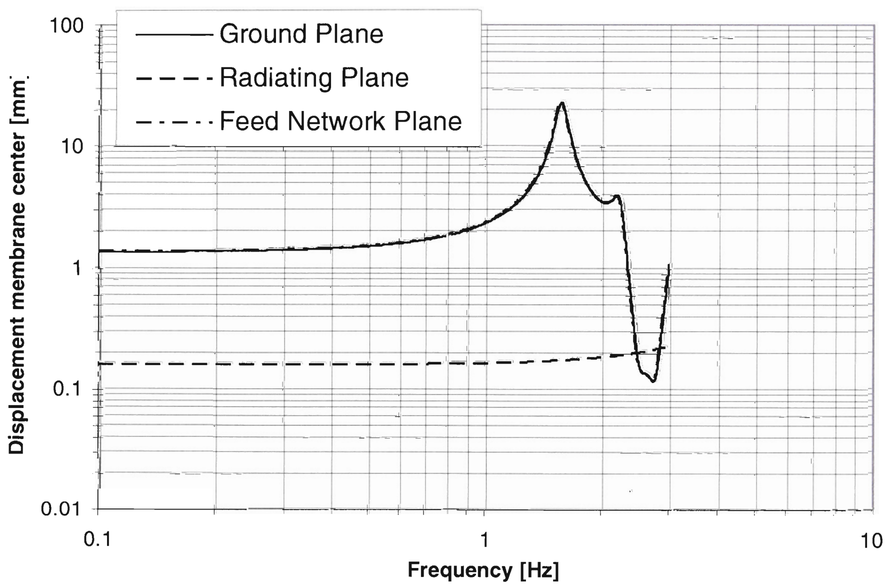
Ground Plane
Radiating Plane
Feed Network Plane
Displacement membrane center [mm]
100
10
1
0.1
0.01
0.1
1
10
Frequency [Hz]

b) Q= 15

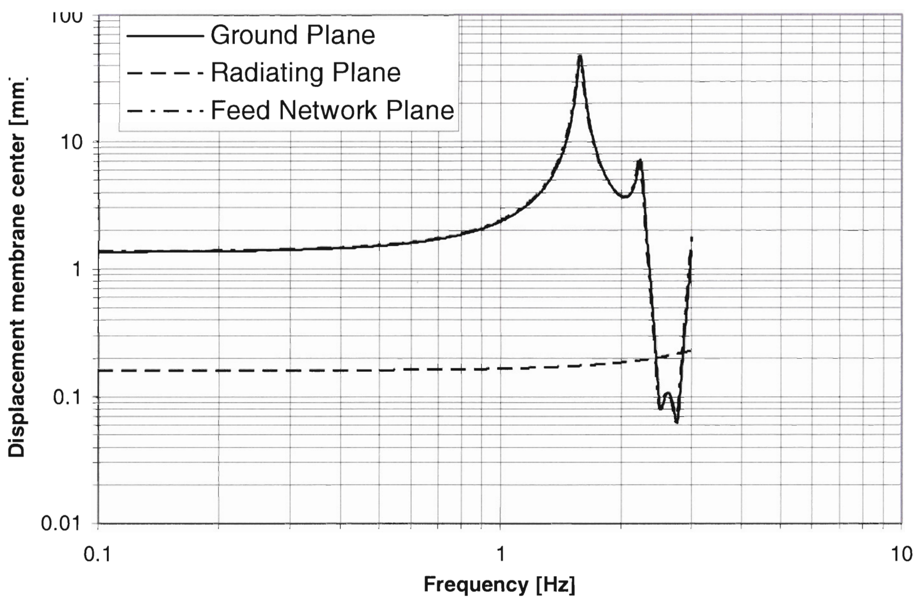

c) Q=30

Figure 7-4 : Dynamic response of the L-Band configuration for an excitation of 0.01 g and different quality factors

Layer	Quality Factor Q	Maximum Displacement [mm]	Frequency of Maximum Displacement [Hz]
Radiating Plane	5	0.851[1]	5.465[1]
Ground Plane		7.862	1.574
Feed Network Plane		7.944	1.565
Radiating Plane	15	2.552[1]	5.505[1]
Ground Plane		23.820	1.582
Feed Network Plane		24.069	1.574
Radiating Plane	30	5.104[1]	5.510[1]
Ground Plane		47.695	1.582
Feed Network Plane		48.194	1.574

1: Results are outside the 0-3 Hz range

Table 7-3 : Dynamic response of the L-Band configuration for different quality factors

Table 7-3 displays the results for the maximum displacements for all layers and the frequency at which they occur. The Radiating Plane maximum displacement occurs outside the 0-3 Hz range as expected since its first natural frequency is at 5.5 Hz. The analysis uses a constant excitation level for all frequencies, even above 3 Hz where it should actually decrease rapidly. For this reason, the Radiating Plane does not generate any concern with its first natural frequency at 5.5 Hz for any damping value.

The dynamic amplifications of the Ground and Feed Network Planes result in maximum displacements outside the 10 mm tolerance for the values of the quality factor Q at 15 and 30. For this shape design and wavelength configuration, a Q greater than 5 leaves the antenna inoperative at all times.

7.4.2 C-Band Membrane Configuration

The out-of-plane displacement tolerance for the C-Band antenna is 2.5 mm as seen in Table 2-9.

All values of Q result in deformations outside the tolerance limit for all layers except the Radiating Plane because its first natural frequency is higher than the 3 Hz threshold. A value of 5 for Q results in the lowest maximum out-of-plane displacements for the Ground and Feed Network Planes at 4.473 mm and 4.793 mm, respectively. These displacements for a Q = 5 are almost twice the tolerance limit. Hence, the membrane shape design for the C-Band configuration has to be completely re-evaluated before it can be integrated on a satellite.

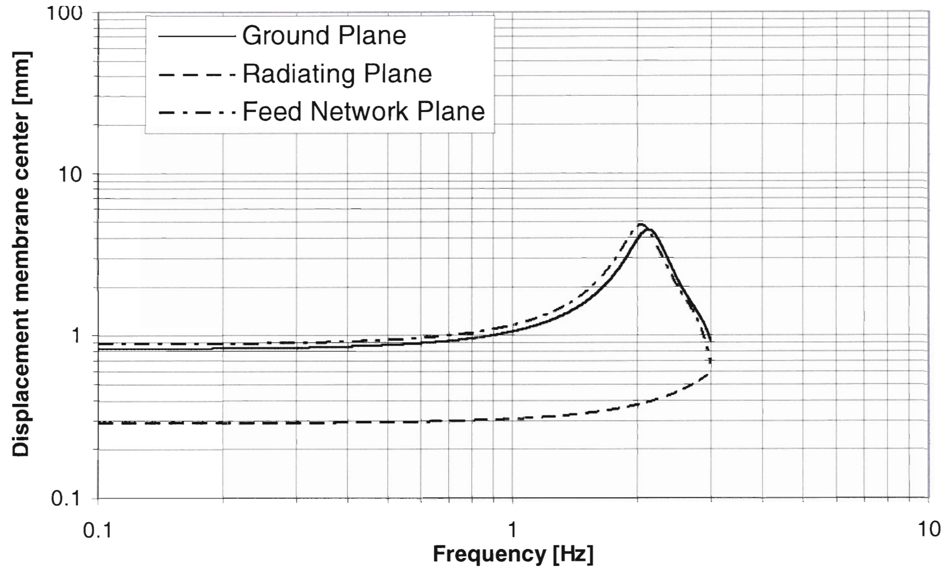
Ground Plane
Radiating Plane
Feed Network Plane
Displacement membrane center [mm]
Frequency [Hz]
100
10
1
0.1
0.1
1
10

a) Q = 5

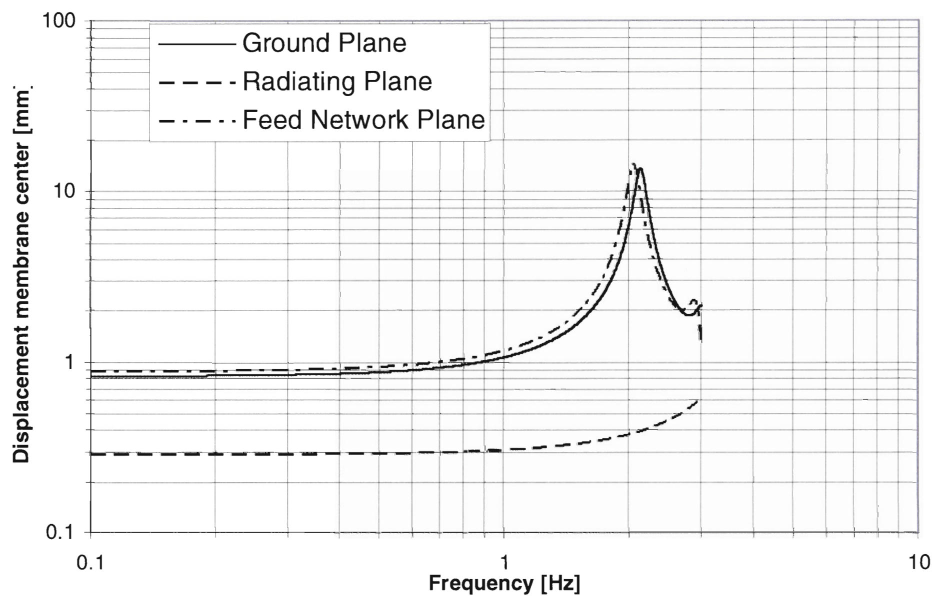
Ground Plane
Radiating Plane
Feed Network Plane
Displacement membrane center [mm]
Frequency [Hz]
100
10
1
0.1
0.1
1
10

b) Q= 15

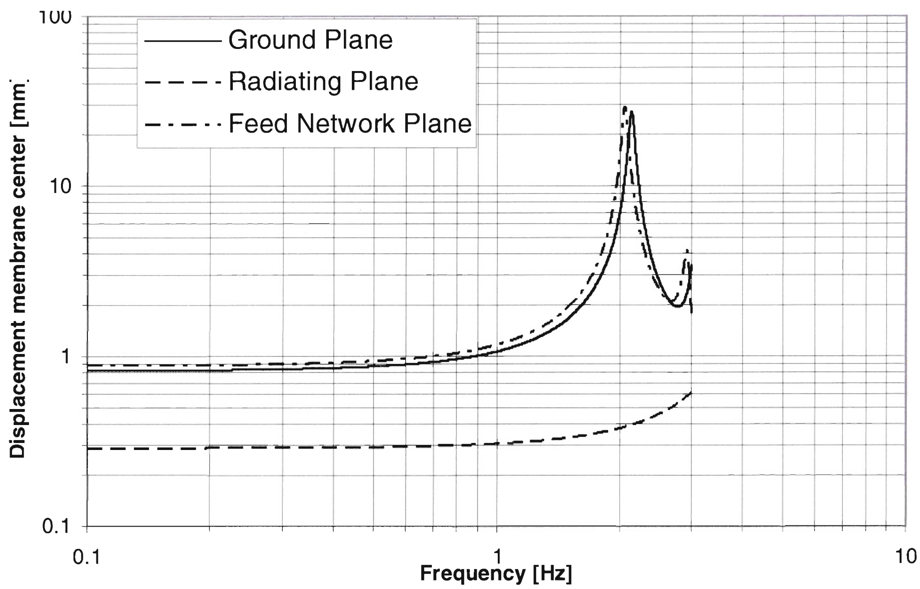

c) Q=30

Figure 7-5 : Dynamic response of the C-Band configuration for an excitation of 0.01 g and different quality factors

Layer	Quality Factor Q	Maximum Displacement [mm]	Frequency of Maximum Displacement [Hz]
Radiating Plane	5	1.453[1]	4.06[1]
Ground Plane		4.473	2.12
Feed Network Plane		4.793	2.04
Radiating Plane	15	4.341[1]	4.103[1]
Ground Plane		13.523	2.133
Feed Network Plane		14.494	2.052
Radiating Plane	30	8.677[1]	4.107[1]
Ground Plane		27.072	2.133
Feed Network Plane		29.014	2.053

1 Results are outside the 0-3 Hz

Table 7-4 : Dynamic response of the C-Band configuration for different quality factors

The dynamic response of the membrane for both wavelength configurations must be lowered. Raising the in-plane tension value would achieve this objective by increasing the stiffness and the first natural frequency above the 3 Hz threshold for all layers. The excitation level dynamically amplified by the membrane would then be less than the current 0.01 g.

Reducing the copper mass on the layers also increases the natural frequencies, although examination of electrical implications is required.

It is critical to determine the quality factor Q accurately. As seen for the L-Band configuration, only one of three factors studied results in an acceptable design. As for the C-Band configuration, the membrane shape design cannot be used as proposed. The results of the frequency response analyses for the 2.25 m x 10 m proposed model show this design to create dynamic displacements outside the allowable tolerance. A full redesign should be considered.

Since micro-vibrations occur during the entire operational life cycle of a satellite, and since a membrane antenna design is particularly vulnerable to dynamic amplification by its large shape and low bending stiffness, the dynamic analyses are critical in the early design stages.

8 TENSIONING SYSTEM REDESIGN AND ANALYSIS

The tensioning system initial design and concept are wholly from EMS Technologies. The design is used on the 2.25 m x 5 m prototype with a cable axial load of 44.48 N. The collaboration for this project brought the redesign of the tensioning system into the work scope of this thesis. The parts have therefore been analyzed with finite element models and redesigned for weight reduction. The tensioning system redesign focuses on the proposed 2.25 m x 10 m model with an increased cable load to 355.85 N. All data and design constraints come from EMS Technologies [17][19].

The purpose of the cable tensioning system is primarily to apply an axial load on the cables, as well as connecting the membrane to the support structure. The membrane antenna is only supported and attached through its tensioning mechanisms. Therefore, this system could represent a failure point of the antenna design and must be closely analyzed.

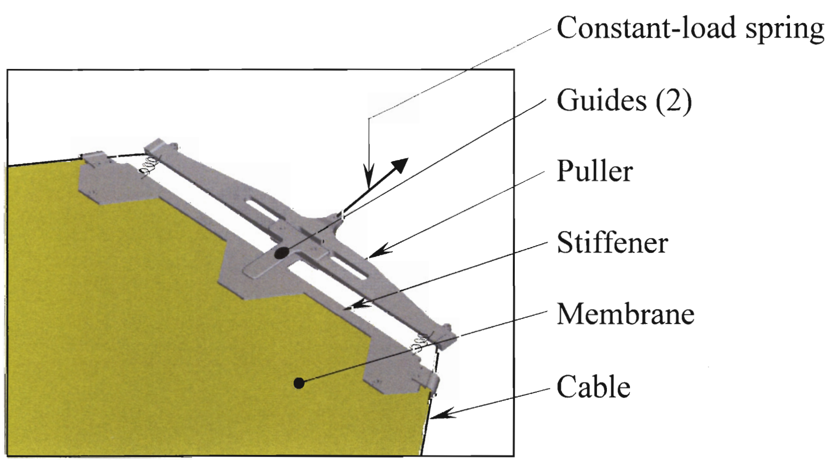

Figure 8-1 : Redesigned tensioning mechanism

The current tensioning system (not shown by the request of EMS Technologies) used on the 2.25 m x 5 m prototype was initially designed without adequate stress analysis [17]. Figure 8-1 illustrates the mechanical concept of this design. A plate called the stiffener is bonded to the membrane along the corner cut-off edge. A part called the puller, pulled by a constant-load spring transmits the correct load onto both cables. Square plates act as guides for the deployment phase. Two smaller springs prevent the guiding square plates from over-extending in the deployment phase, or twisting during folding and storage risking tear.

The design has one part, the puller, with a non-negligible stress field. It is analyzed in this chapter with the increased cable axial load and the required spring load.

The analysis presented in this chapter does not consider any temperature variations.

8.1 Assumptions for the Tensioning Mechanism

- It is assumed that the cable loads are effectively replaced on the puller by an equivalent distributed load on the interior surface of their connection holes.
- The parts of the tensioning mechanism are assumed to be made of aluminium 7075-T6.
- The parabolic shape of the cable remains unchanged when the tensioning load is applied. The design should yield the desired parabolic shape when fully stretched.

8.2 Details of the Finite Element Modeling

The 2.25 m x 5 m model has a cable load of 44.48 N, but the 2.25 m x 10 m model requires a cable load of 355.85 N. The puller needs to be reviewed for this increase in load. All other parts are redesigned to decrease the total weight without any structural analysis.

The modelling and modification of the design are made with the Pro-Engineer software. The masses of the parts are determined using this software. The design is exported into MSC.Patran for the meshing of the part. The analysis uses tetrahedral solid elements. Figure 8-2 details the boundary conditions and applied loads. The aluminium 7075-T6 properties are used. A static analysis is conducted using MSC.Nastran.

8.3 Design Requirements Overview

The purpose of this tensioning system is twofold: tensioning the cables and connecting the membrane to the support structure through the spring. The deployment phase and the unfolding phase bring unique constraints.

The puller and the stiffener must be kept close and aligned to prevent membrane tear in the deployment phase where movement and stretching occur. Both the guides and the smaller springs carry out these functions.

The puller transmits the load from the constant-load spring to the cables. The stiffener provides corner rigidity for the storage and deployment phase.

8.4 Modifications and Optimization

The initial design uses 4 square guides. Their size, shape and number are reduced. The 2 reviewed guides, smaller and of different shape are shown in Figure 8-1. The stiffener has been cut for weight reduction at the centre of the part, except for the region interacting with the guides as illustrated in the same figure. The details of the modifications are not presented since finite element optimization or other types of calculations have not been used in the redesign of these parts.

The puller is subjected to a finite element analysis for resizing and weight optimisation. This part appears 12 times in the antenna design (4 per layer, 3 layers per antenna). Each gram saved becomes important, especially considering this type of antenna is studied for its lightweight characteristics.

A static analysis is performed for this part. The dynamic analysis of the membrane reveals that 0.007 N is added to the total cable load by dynamic behaviour of the membrane. Considering that the cable is already preloaded to 356 N, the impact of the dynamic behaviour is considered negligible.

The basic length of the part is not modified from the initial design because the length of the corner cut-off edge is identical for the 2.25 m x 5 m and the 2.25 m x 10 m models at 10 inches (0.254 m). The thickness and width of the part have increased considerably.

Since curvature is present, and hence stress concentration, the meshes around these areas are refined.

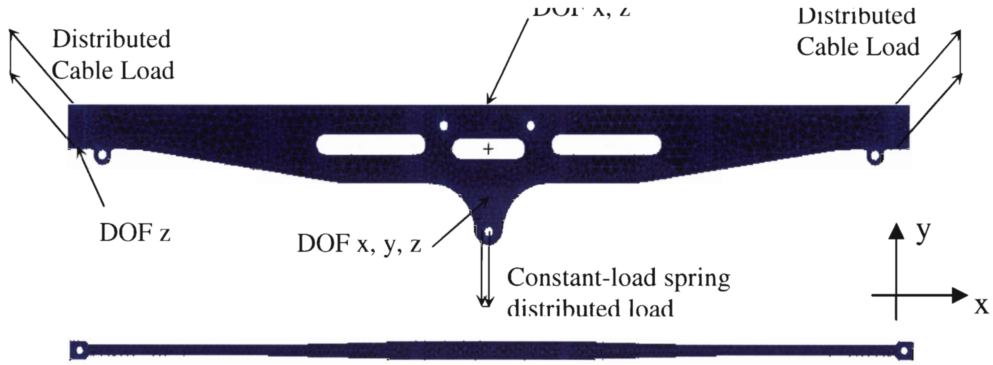

Figure 8-2 : Boundary conditions and loads for the puller

As displayed in Figure 8-2, the loads are included as equivalent distributed loads over the interior surfaces of the cables or spring connection holes preventing stress concentrations. This substitution represents closely the design purpose of connecting the constant-load spring to the puller with a bolt and nut. This fastening method transforms the spring load into an equivalent pressure on the interior surface of the hole. The cable axial loads are replaced in a similar fashion by distributed loads. These distributed loads are implemented in the model at a calculated angle on the interior surface of the connection holes as shown in Figure 8-2, preventing stress concentration occurrence.

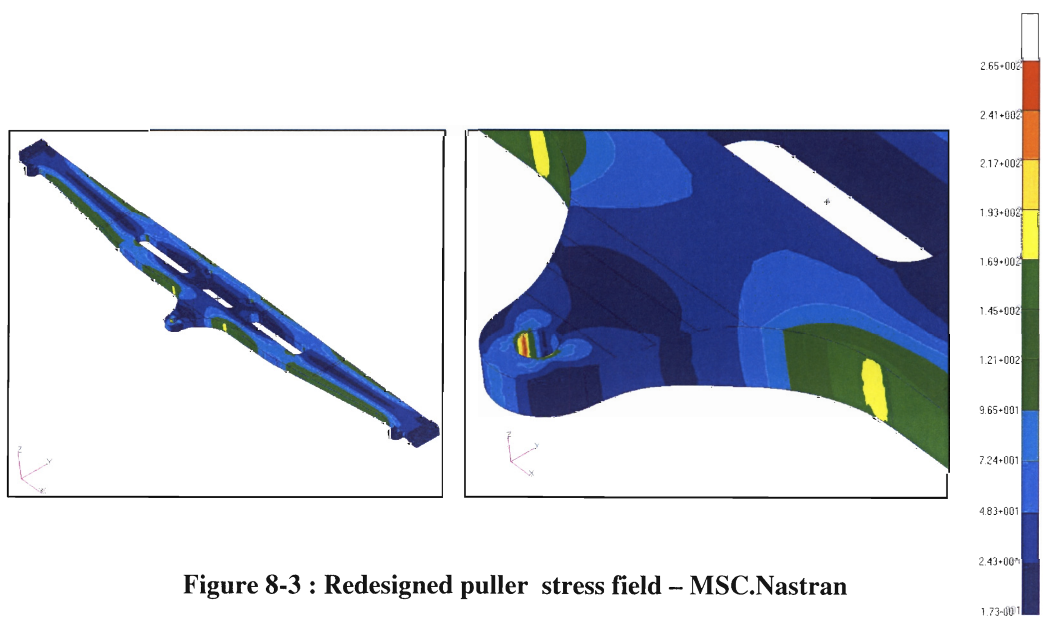

Figure 8-3 : Redesigned puller stress field – MSC.Nastran

Design iterations are needed and were carried out. The results shown in Figure 8-3 give a desired and comfortable security factor of 1.9. The tensile yield strength of the aluminium 7075-T6 is 503 MPa [15] and the maximum stress obtained with the finite element analysis is 265 MPa.

This redesign of the tensioning system allows a considerable decrease in weight. Each gram saved in the redesign of one part represents a reduction of 12 grams for the antenna.

Part	Original Design Part Weight [kg]	Redesigned Part Weight [kg]	Total Design Weight Variation [kg]
Stiffener	0.255	0.184	-0.071
Puller	0.214	0.259	+0.045
Guides	0.340	0.058	-0.282
Total (12 corners)	9.708	6.012	**-3.696**

Table 8-1 : Weight reduction with redesigned tensioning system

The total reduction in weight for the whole antenna is 3.696 kg. Each kilogram costs thousands of dollars to launch on a satellite mission. The puller has a slight increase in its weight but is now designed for a cable load of 355.85 N instead of 44.48 N.

9 CONCLUSION

The main purpose of this thesis was to look ahead into the next steps in the development of a novel membrane antenna technology and to develop tools to overcome anticipated obstacles on the mechanical engineering side of the project.

The impact of the parabolic shapes on the cable axial load and its consequent impact on the antenna support structure are studied. Some trade-off decisions have been underlined and engineering suggestions clearly emphasized.

Also, the wrinkling characteristic of the membrane layer had to be the object of particular attention since wrinkles can greatly affect the functionality of the antenna. Numerical tests on a complex model, such as the 2.25 m x 5 m prototype modeled in Abaqus, were carried out with tensile loads using a recently suggested finite element approach. Once proved that the approach could handle more complex models, thermal loads were incorporated into the finite element analyses. Thermal loads are expected to generate wrinkle pattern on the membrane antenna while in-orbit.

Controlling the wrinkles formed under temperature variations represents an interesting engineering aspect of the membrane antenna design. Features controlling wrinkles could allow reducing the global size of the antenna by allowing engineers to bring closer the corner cut-off edges to the central electrical aperture while also reducing the total weight of the mission.

Considering the sensibility to vibrations, the flexibility and the size of the proposed 2.25 m x 10 m antenna, a dynamic analysis was carried out to shed light on the behaviour of the antenna subjected to on-orbit micro-vibrations. Both L-Band and C-Band wavelength configurations were analyzed.

Collaboration with EMS Technologies brought into the work scope the need to redesign the corner tensioning system to accommodate the proposed antenna dimensions and required cable loads.

9.1 Summary of Findings

The membrane shape study, wrinkles analysis considering thermal variations and dynamic analysis are all interlocked. All must be done to fully accept a design, but only one is sufficient to reject it.

9.1.1 Membrane Shape and Cable Load

The equation governing the axial load of the cable stretching the membrane shows that it does not vary proportionally to the d/ℓ ratio (depth over length) of the parabolas but to the square root of an expression containing the inverse of this ratio.

A study is conducted by varying the shapes of the side's parabola, and analysing the variation of the resulting total area and cable load while considering the cutting process of the corners. The study revealed that, for an increase of the membrane surface, a decrease in cable axial load and therefore transmitted load to the support structure is obtained, but the load tends to stabilize for an even larger surface area. This is consistent with the derived equation governing the axial load of the cables.

An increase in the membrane size has the effect of requiring a larger support structure but it also results in a lower cable load. The lower cable load means that the support structure has a lower required stiffness. Both these impacts on the support structure influence its weight in opposite fashion and in different proportion. When the type of support structure for the antenna is defined by the manufacturer, this study will be able to quantify the impact of the support structure to determine an optimum design.

9.1.2 Wrinkling Analysis

The random imperfection method for the finite element wrinkling analysis incorporates adequately complex shape and multiple tensile loads. The finite element analyses with thermal loads show that thermal loads can be considered with the random imperfection method, opening up a new spectrum of possibilities of analyses necessary for eventual flight design. Definite conclusions can only be drawn by corroboration with experimental results. The necessary resources were not available to conduct experiments. The numerical results obtained, however, are consistent with intuitive expectations.

9.1.3 Wrinkling Analysis with Thermal Loads

Heating a central surface of a stretched rectangular membrane results in wrinkles over that heated area oriented in the correct direction. The cooled central region, contracting the affected area, produces major wrinkles between its corners and the loads stretching the membrane as expected.

The thermal loads, representing space environment on the 2.25 m x 5 m finite element model, shows that complete exposure to solar radiations or a situation completely in the Earth shadow, results in wrinkle formation concentrated in the corners. The corner wrinkles for these cases are outside the electrical aperture, therefore acceptable.

The results from simulating the shadow of the satellite onto the antenna membrane layers show wrinkles forming inside the electrical aperture affecting a considerable area. The height of the wrinkles is well within electrical planarity tolerance for the 2.25 m x 5 m model with the L-Band wavelength. Other designs of the membrane or wavelengths used could possibly result in out-of-plane deformations outside the tolerance limit.

9.1.4 Controlling Wrinkles

Controlling the height and orientation of the wrinkles occurring on the membrane can be accomplished using a passive approach. The feasibility of such design has been shown by demonstrating that the pattern, orientation and height of the wrinkles can be modified. One design showed a reduction in the wrinkle height, while another design controlled the extent of the area affected by wrinkles. Such designs can allow engineers to bring the corner cut edges closer to the electrical aperture. This would reduce the total antenna size, and at the same time reduce its weight as well as its support structure's weight.

9.1.5 Dynamic Analysis

Dynamic analysis shows that the behaviour of the 2.25 m x 10 m model subjected to on-orbit micro-vibrations is dependent on the true damping value of the design. A quality factor (Q) of 5, i.e. damping ratio of 0.1, results in an out-of-plane maximum displacement within the specified tolerance for the L-Band configuration. All other values of Q considered result in a displacement outside the tolerance. Similarly, the C-Band configuration has, for all damping ratios, a maximum displacement outside the tolerance limit. Therefore, for the C-Band and for most Q values of the L-Band configuration, the antenna, as it stands now, cannot be used for a SAR mission. Increasing the in-plane tension to a higher value altering the first natural frequency, could correct this issue.

9.2 Suggestions for Further Work

Once the support structure of the membrane antenna is chosen, a study can quantify the trade-off for optimum antenna size, cable load and support structure weight.

A comparison of results of finite element analysis and experimental tests is needed to validate the random imperfection approach. In the numerical analysis, gravity should be included if the experimental test setup is subjected to it.

Manufacturing issues force the membrane to be composed of multiple bonded sheets of polyimide material to form the full layer. The impact of the bonded joints and the bonding method should be taken into consideration in the future models.

The dynamic analysis should include the temperature variation since the stiffness of the membrane, affected by this variation, changes the natural frequency of the design.

REFERENCES

1 : Canadian Space Agency web site: http://www.space.gc.ca.

2 : Nature Publishing Group web site: http://www.nature.com/news/2005/050103/multimedia/050103-2-m1.html.

3 : Wagner, H., *Flat Sheet Metal Grinder with Very Thin Metal Web*, Zeitschrift für Flugtechnik Motolurftschiffahrt, 1929.

4 : Reissner, E., *On Tension Field Theory*, Proc. V Int. Cong. Appl. Mech., pages 88-92, 1938.

5 : Mansfield, E. H., *Tension Field Theory, A New Approach which Shows its Duality with Inextensional Theory*, Proc. XII Int. Cong. Appl. Mech., pages 305-320, 1968.

6 : Stein, M., Hedgepeth, J. M., *Analysis of Partly Wrinkled Membranes*, NASA TN D-813, 1961.

7 : Miller, R. K., Hedgepeth, J.M., *An Algorithm for Finite Element Analysis of Partly Wrinkled Membranes*, AIAA, 20:1761-1763, 1982.

8 : Adler, A. L. Mikulas, M. M., Hedgepeth, J. M., *Static and Dynamic Analysis of Partially Wrinkled Membrane Structures*, 41st AIAA/ASME/ASCE/AHS/ASC Structures, Structures Dynamics, and Material Conference and Exhibit, Atlanta, GA. AIAA-2000-1810.

9 : Wong, Y. W., Pellegrino, S., *Wrinkled membranes. In: Textile Composites and Inflatable Structures*, E. Onate and B. Kroplin, eds., CIMNE, Barcelona, 2003.

10 : Wong, Y. W., Pellegrino, S. and Park, K. C., *Prediction of wrinkle amplitudes in square solar sails*. In Proc. 44th AIAA/ASME/ASCE/AHS/ASC Structures,

Structural Dynamics and Materials Conference, 7-10 April 2003, Norfolk, VA AIAA 2003-1982

11 : Wong, Y. W., Pellegrino, S., *Computation of wrinkle amplitudes in thin membranes.* In Proc. 43rd AIAA/ASME/ASCE/AHS/ASC Structures, Structural Dynamics and Materials Conference, 22-25 April 2002, Denver, CO, AIAA 2002-1369.

12 : Wong, Y.W., Pellegrino, S.. *Amplitude of wrinkles in thin membranes.In:New Approaches to Structural Mechanics,Shells and Biological Structures* ,edited by H.R.Drewand S.Pellegrino.Kluwer Academic Publishers,257-270, 2002.

13 : Tessler, A., Sleight, D.W., Wang, J.T., *Nonlinear Shell Modeling of Thin Membranes With Emphasis on Structural Wrinkling*, AIAA 2003-1931; 44th AIAA/ASME/ASCE/AHS/ASC Structures, Structural Dynamics, and Materials Conference, Norfolk, Virginia, April 7-10.

14 : *Dupont™ Kapton® E High Modulus Polyimide Film*, Technical Information, H-97928, 2003.

15 : Material Data Resources web site: http://www.matweb.com.

16 : *DuPont™ Pyralux® AP All-Polyimide Flexible Laminate*, Technical Information, H-73241-2, 2001.

17 : Private Communications, EMS Technologies.

18 : Private Communications, Dr. Xin Xiang Jiang and Dr. Marie-Josée Potvin, Canadian Space Agency.

19 : Arthur Baylis, Gérard Carrier, Minya Gavrilovi, Dino Kefallinos, Luis Matrins Camelo, Karima Nasri, Stephen Wilson, *Membrane Antenna Prototype Development – Final Report*, EMS Technologies, Internal Report Number RML-009-2003-138, 286 pages.

20 : Krenck, S., *Mechanics and Analysis of Beams, Columns and Cables*, 2nd edition, Springer, Berlin, 2001.

21 : Gimsing, Neils J., *Cable Supported Bridges: Concepts and Design*, 2nd edition, John Wiley and Sons, New York, 1997.

22 : Lee, Sang H., *MSC/Nastran Handbook for Nonlinear Analysis*, version 67, The MacNeal-Schwendler Corporation, Los Angeles, 1992.

23 : MSC/NASTRAN User's Guide, Version 70.5, *Quick Reference Guide*, The MacNeal-Schwendler Corporation, Los Angeles, 1994

24 : Shigley, Joseph E., Mischke, Charles R., *Mechanical Engineering Design*, 5th edition McGraw-Hill, New York, 1989.

25 : Yang, B., Ding, H., Lou, M., and Fang, H., *A New Approach to Wrinkling Prediction of Space Membrane Structures*, presented at the AIAAGossamer Spacecraft Forum, the 42nd AIAA/ASME/ASCE/ASC Structures, Structural Dynamics, and Materials Conference, Seattle, WA, April 16-19, 2001.

26 : H. Ding and B. Yang M. Lou and H. Fang, *A Two-Viable Parameter Membrane Model For Wrinkling Analysis of Membrane Structures*, AIAA 2002-1460.

27 : Blandino, J.R., Johnston, J.D., Dharamsi, Urmil K., J.S., *Corner Wrinkling of a Square Membrane Due to Symmetric Mechanical Loads*, Journal of Space craft and Rockets, Vol. 39, No. 5, September-October 2002.

28 : Blandino, J.R., Johnston, J.D., Miles, J.J., Soplop, J.S., *Thin Film Membrane Wrinkling due to Mechanical and Thermal Loads*, 42nd AIAA/ASME/ASCE/AHS/ASC Structures, Structural Dynamics, and Materials Conference, 16-19 April 2001, Seattle, WA, AIAA 2001-1345.

29 : Incropera, Frank P., DeWitt, David P., *Fundamentals of Heat and A Mass Transfer*, 4th edition, Wiley, New York, 1996.

30 : Meirovitch, Leonard, *Fundamentals of Vibrations*, 1st edition, McGraw-Hill, New-York, 2001.

31 : Cook, Robert D., Malkus, David S., Plesha, Michael E., Witt, Robert J., *Concepts and Applications of Finite Element Analysis*, 4th edition, Wiley, New York, 2002.

32 : Buchanan, George R., *Schaum's Outline of Theory and Problem of Finite Element Analysis*, McGraw-Hill, New York, 1995.

33 : Spiegel, Murray R., *Formules et tables de mathématiques*, Série Schaum, McGraw-Hill, New-York, 1974.

34 : *ABAQUS/Standard User's Manual, Version 6.3.1*, Hibbitt, Karlsson, and Sorensen, Inc., Pawtucket, RI, 2002.

APPENDIX A. CALCULATIONS OF THE CORNER CUT-OFF WITH DISTANCE *K* CONSTANT

The corner cut-off position and orientation using the distance k constant from the electrical aperture corner to the corner cut-off shown in Figure 3-3-(b), are obtained with different mathematical equations since the constrainsts on the design are slightly different. The mathematical set of six equations for six unknowns (x_m, y_m, x_1, y_1, x_2, y_2) are as follow:

$$k^2 = \left(y_m - {l_a}/{2} \right)^2 + \left(x_m - {l_o}/{2} \right)^2 \qquad \textbf{A.1}$$

$$\frac{y_m - l_a/2}{x_m - l_0/2} = \frac{2Ax_1 + 1}{1 + 2Cy_2} \qquad \textbf{A.2}$$

$$y_1 = Ax_1^{\ 2} + B \qquad \textbf{A.3}$$

$$x_2 = Cy_2^{\ 2} + D \qquad \textbf{A.4}$$

$$\frac{y_2 - y_1}{x_2 - x_1} = \frac{l_0/2 - x_m}{y_m - l_a/2} \qquad \textbf{A.5}$$

$$\frac{{l_2}/{2} - \frac{y_1 + y_2}{2}}{{l_1}/{2} - \frac{x_1 + x_2}{2}} = \frac{2Ax_1 + 1}{1 + 2Cy_2} \qquad \textbf{A.6}$$

Equations A.2 and A.6 both describe the parallelism of two lines (four lines in all) perpendicular to the corner cut-off edge. Two of these lines and their perpendicularity to the corner edge are illustrated in Figure 3-3. Equation A.2 outline the parallelism between the first line from the electrical aperture corner to the closest point on the edge (x_m, y_m) and a second line from the midpoint of the corner edge parallel to the resultant of the vectors summation of the cable loads T_1 and T_2. Equation A.6 describes a similar constraint.

This set of equations using the distance *k* is non-linear and coupled as with the set used with the other method. Solving it analytically proved difficult even with the help of specialized software.

APPENDIX B. CALCULATION OF THE MEMBRANE TOTAL AREA

A geometric method for evaluating the area is chosen by adding and subtracting different subsections specifically chosen for simplifying the calculations as shown below and in Figure B-1. The area subsections are described as follow:

$$A_{TOT} = 4A_1 - (4A_2 - 4A_3) = 4A_1 + 4A_3 - 4A_2$$

$$A_1 = \int_0^{l_1/2} \left(\frac{F_1}{2H_1 \cdot l_1} x^2 + \frac{l_2}{2} + d_1 \right) dx = \frac{F_1 \cdot l_1^{\,2}}{48H_1} + \frac{l_1}{2} \cdot \left(\frac{l_2}{2} - d_1 \right) \qquad \textbf{B.1}$$

$$A_2 = \frac{l_1 \cdot l_2}{4} \qquad \textbf{B.2}$$

$$A_3 = \int_0^{l_2/2} \left(\frac{F_2}{2H_2 \cdot l_2} y^2 + \frac{l_1}{2} + d_2 \right) dy = \frac{F_2 \cdot l_2^{\,2}}{48H_2} + \frac{l_2}{2} \cdot \left(\frac{l_1}{2} - d_2 \right) \qquad \textbf{B.3}$$

$$A_{TOT} = \frac{F_1 \cdot l_1^{\,2}}{12H_1} + \frac{F_2 \cdot l_2^{\,2}}{12H_2} + l_1 \cdot l_2 - 2l_1 \cdot d_1 - 2l_2 \cdot d_2 \qquad \textbf{B.4}$$

To simplify the upcoming calculation of the corner cut area, the following substitutions are used:

$$\frac{F_1}{2H_1 \cdot l_1} = A \qquad \frac{l_2}{2} - d_1 = B \qquad \frac{F_2}{2H_2 \cdot l_2} = C$$

$$\frac{l_1}{2} - d_2 = D \qquad y_1 - \left(\frac{y_2 - y_1}{x_2 - x_1} \right) \cdot x_1 = b \qquad \frac{y_2 - y_1}{x_2 - x_1} = m$$

B.5

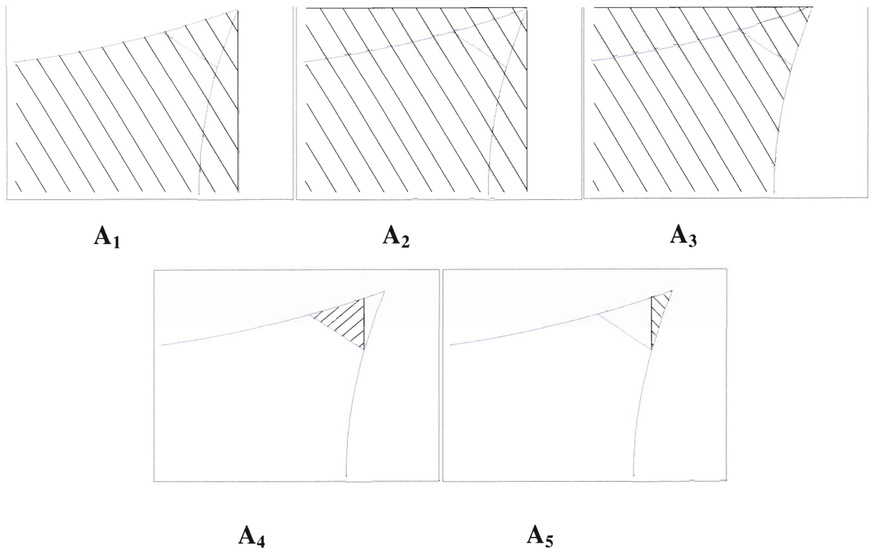

Figure B-1 : Area calculation subsection division

The area cut is divided into two different areas chosen for the ease of integration as seen in Figure B-1-(A_4) and (A_5).

$$A_4 = \int_{x_1}^{x_2} \left(A\cdot x^2 + B - m\cdot x - b\right)\cdot dx \;=\; \frac{A}{3}\cdot\left(x_2^{\,3} - x_1^{\,3}\right) - \frac{m}{2}\cdot\left(x_2^{\,2} - x_1^{\,2}\right) + (B-b)\cdot(x_2 - x_1) \qquad \textbf{B.6}$$

$$A_5 = \int_{x_2}^{\frac{l_1}{2}} \left(A\cdot x^2 + B - \sqrt{{(x-D)}/{C}}\right)\cdot dx$$

$$A_5 = \frac{A}{3}\cdot\left(\frac{l_1^{\,3}}{8} - x_2^{\,3}\right) + B\cdot\left(\frac{l_1}{2} - x_1\right) - \frac{2C}{3}\cdot\sqrt{\left(\frac{l_1/2 - D}{C}\right)^3} + \frac{2C}{3}\cdot\sqrt{\left(\frac{x_2 - D}{C}\right)^3} \qquad \textbf{B.7}$$

Subtracting the results of equations B.6 and B.7 from the total area found in equation B.4 yields the accurate total area:

$$A_{MECH} = 4\cdot\left(A_1 + A_3 - \left(A_2 + A_4 + A_5\right)\right) \qquad \textbf{B.8}$$

APPENDIX C. CALCULATIONS FOR THE WIRES AND STRIPS OF THE WRINKLE CONTROL FEATURES

The passive designs require wires, or band strips, connected to the holes or slots cut on the membrane on one end and attached to the aluminium plate on their other end. The temperature gradually initiates a volume decrease on the wire or strip generating the desired load. This load at -40°C is 0.05 N. The corresponding diameter, or width, is calculated for different materials as seen in Table C-1 and Table C-2.

For a straight bar restricted at both ends and subjected to a temperature variation, the thermal stress σ is function of the strain ε and the Young's modulus E. The strain is calculated with the coefficient of thermal expansion α and the temperature variation ΔT [24]:

$$\sigma = \varepsilon \cdot E = \alpha(\Delta T)E \qquad \textbf{C.1}$$

In a similar manner, for a uniform flat plate restrained at the edges and subjected to a uniform temperature variation, the thermal stress developed is [24]:

$$\sigma = \frac{\alpha(\Delta T)E}{1-\upsilon} \qquad \textbf{C.2}$$

The resulting area is extracted by:

$$A = \frac{F}{\sigma} \qquad \textbf{C.3}$$

The diameter of the wire is calculated with the load F of 0.05 N. For the strips linking the corner aluminium plate to the membrane holes or slots, a thickness of 0.0005 in (0.0127 mm) is used for calculating the section width.

The required wire diameters are presented in Table C-1 for different material properties [15].

Material	Diameter [mm (in)]
Aluminium 7075-T6	0.0242 (0.00095)
Aluminium 6061-T6	0.0255 (0.00101)
Copper	0.0242 (0.00095)
Titanium	0.0301 (0.00118)
ABS Polymer	0.0490 (0.00193)
Nylon	0.0502 (0.00198)

Table C-1 : Wire diameter for different material properties for the wrinkle control feature designs

The solutions of using metal materials result in wire diameters equivalent to a few hair strands. They do not represent a practicable solution to physically implement on the membrane. The non-metal materials suggested in Table C-1, while resulting in a larger diameter cannot be considered for the membrane either. The possibility of using a wire in the wrinkle control feature designs is impracticable for the material studied.

The results of the calculations for the width of strips calculated for different material properties [15] are summarized in Table C-2.

Material	Width [mm (in)]
Aluminium 7075-T6	0.024 (0.0096)
Titanium	0.037 (0.0015)
Polyimide 2 material	0.519 (0.0204)
Polyamide-Imide	0.241 (0.0094)
Nylon	0.101 (0.0040)

Table C-2 : Strip width for different material properties for the wrinkle control feature designs

All metal solutions are impracticable for physical implementation on the membrane.

The polyimide 2 material represents the ideal choice for the strips. Its width of 0.5 mm is physically possible to implement on the membrane. Also, it is the same material as the membrane itself therefore pieces of material leftover from the membrane manufacturing should be available. An extensive search into all possible materials would possibly reveal better choices.

A different membrane shape design with a higher in-plane tension would require a higher load used for these control features yielding larger sections of the wires or strips. This would offer more choices for possible materials.

The wrinkle control feature designs discussed in this thesis add negligible mass and represent a passive control method. At the same time, it offers the possibility of reducing the membrane size as well as the size and weight of the support structure.